The Impact of System Effects on Estimates of Faraday Rotation From Synthetic Aperture Radar Measurements

Shaun Quegan, *Member, IEEE*, and Mark R. Lomas

***Abstract*—Radio waves traversing the Earth's ionosphere suffer from Faraday rotation with noticeable effects on measurements from lower frequency space-based radars, but these effects can be easily corrected given estimates of the Faraday rotation angle, i.e., Ω. Several methods to derive Ω from polarimetric measurements are known, but they are affected by system distortions (crosstalk and channel imbalance) and noise. A first-order analysis for the most robust Faraday rotation estimator leads to a differentiable expression for the bias in the estimate of Ω in terms of the amplitudes and phases of the distortion terms and the covariance properties of the target. The analysis applies equally to L-band and P-band. We derive conditions on the amplitudes and phases of the distortion terms that yield the maximum bias and a compact expression for its value for the important case where $\Omega = 0$. Exact simulations confirm the accuracy of the first-order analysis and verify its predictions. Conditions on the distortion amplitudes that yield a given maximum bias are derived numerically, and the maximum bias is shown to be insensitive to the amplitude of the channel imbalance terms. These results are important not just for correcting polarimetric data but also for assessing the accuracy of the estimates of the total electron content derived from Faraday rotation.**

***Index Terms*—Calibration, Faraday rotation, ionospheric structure, radar imaging, radar polarimetry.**

I. Introduction

THE presence of the geomagnetic field causes radio waves traversing the Earth's ionospheric plasma to suffer from Faraday rotation, which rotates the plane of polarization of the propagating wave through an angle given by [1, p. 343]

$$\Omega = \frac{e^3}{8\pi^2 \varepsilon_0 m^2 c} \frac{B \cos\psi}{f_0^2} \mathrm{TEC} \sec\theta \tag{1}$$

where e is the electron charge, m is the mass of the electron, ε_0 is the permittivity of free space, B is the geomagnetic field intensity, f_0 is the radio frequency, ψ is the angle between the radar beam and the geomagnetic field, TEC is the (vertical) total electron content (TEC), and θ is the angle of the ray to the vertical. Studies at L-band (wavelength $\sim$24 cm) have presented the likely variations of Ω under latitude, season, and solar activity variations [2], and they have shown that Ω can take values up to $\pm 20^\circ$ for the large values of the TEC encountered under solar maximum conditions [3]. These calculations can be easily converted to the P-band case (wavelength $\sim$70 cm) since the Faraday rotation scales as wavelength squared [see (1)]; hence it is an order of magnitude greater at P-band than at L-band. If left uncorrected, this would seriously distort the polarimetric measurements to be gathered by the European Space Agency P-band BIOMASS mission [4].

The correction of the Faraday rotation simply involves counterrotating the data once Ω has been measured, which has prompted the development of several algorithms to estimate Ω from polarimetric SAR data [5]–[8]. These estimates are also of interest in their own right since (1) indicates that they allow the TEC to be measured. The sensitivity of the BIOMASS signal to the Faraday rotation will thus enable ionospheric structure and dynamics to be routinely monitored along the satellite's dawn–dusk orbit, which cuts across such important ionospheric features as the midlatitude trough and the auroral oval [9]. Furthermore, proposed methods for correcting scintillation effects in SAR images require accurate estimates of the Faraday rotation [10], [11].

Faraday rotation transfers energy between polarizations and needs to be corrected to better than 5° in order to avoid significant errors in derived geophysical parameters, such as the woody biomass [2], [3]. Meyer and Nicoll [12] suggested a more stringent requirement of 1.2° for accurate applications of polarimetry over a general set of ground cover types. However, three factors affect the accuracy of Faraday rotation estimates as follows.

1) Different estimators give different levels of accuracy depending on the type of distortion. For the published estimators, the best overall performance against a range of metrics (see [13] and [14]) is given by the Bickel and Bates algorithm [5]. In this paper, we therefore exclusively deal with this algorithm.
2) All published algorithms rely on estimating covariance terms for distributed targets; thus, they are subject to the statistical properties of such estimates [15]. However, it is not easy to relate this knowledge to the statistics of Faraday rotation measurements, and simulations are usually required to explore this issue.

Manuscript received April 22, 2014; revised August 22, 2014; accepted November 28, 2014. This work was supported in part by the European Space Agency (ESA) under ESA/European Space Research and Technology Centre (ESTEC) Contract 22849/09/NL/JA/ef, by the U.K. National Environment Research Council through the National Centre for Earth Observation, and by the U.K. Space Agency.

The authors are with the School of Mathematics and Statistics, University of Sheffield, Sheffield S37RH, U.K. (e-mail: s.quegan@sheffield.ac.uk; m.r.lomas@sheffield.ac.uk).

Digital Object Identifier 10.1109/TGRS.2015.2395076

3) Faraday rotation estimates are disturbed by unknown or imperfectly known system distortions. These include crosstalk (caused by undesired coupling between polarizations on both transmit and receive), channel imbalance (which describes the system-induced deviations of the amplitude ratio from unity and the phase difference from zero for the orthogonal polarizations used by the system on both transmit and receive), and noise.

This paper is concerned with the third of these factors and aims to disentangle the complex interaction between system distortions and Faraday rotation. Earlier studies have made partial progress with this problem but were largely based on simulation and made various simplifying assumptions, such as that all crosstalk components were equal or that the crosstalk was reciprocal [6], [8], [16], [17]. Here, instead, we provide an algebraic first-order analysis that illuminates the relative importance of crosstalk, channel imbalance, and noise in degrading the estimates of the Faraday rotation, and that makes clear the role of both the phases and amplitudes of the distortion terms in controlling the bias in these estimates.

Section II takes the system model in [6] as a basis for the analysis and gives the key expressions for polarimetric measurements that have been either calibrated using imperfectly known values of crosstalk and channel imbalance or are left uncalibrated; the underlying details are set out in a companion paper [18]. In Section III, we use these expressions to derive a compact differentiable formula for the bias in the estimated Faraday rotation given the phases and amplitudes of the distortion terms. The bias is shown to depend on particular combinations of the crosstalk and channel imbalance terms and on the covariance properties of the scene. We then exploit this formula to find the conditions under which the maximum bias occurs. In the general case, this leads to equations that do not have simple analytic solutions, but they can be readily solved when the true value of the Faraday rotation is zero. This case is important since the analysis applies not only to P-band but also to L-band, where the Faraday rotation is much smaller; thus, the bias could become significant relative to the mean value of the Faraday rotation. In addition, in order to minimize ionospheric effects, BIOMASS calibration is best performed near the geomagnetic equator where the Faraday rotation is small, but account must still be taken of its deviation from zero. It is also shown in Section V-B that, if the channel imbalance is negligible, the largest biases occur when the Faraday rotation is small.

To test the predictions from the analysis, an exact simulation scheme is also developed, as described in Section IV. This not only confirms the predictions of the analysis but also allows us to derive the statistical properties of the estimation errors as the system distortion and noise vary, as illustrated in Section V. Conclusions are given in Section VI.

II. First-Order Analysis of System Effects

The measured scattering matrix, i.e., $\mathbf{M}$, with Faraday rotation and system errors (channel imbalance, crosstalk, and noise) is given in [6] as

$$\begin{aligned}\mathbf{M} &= \begin{bmatrix} M_{\mathrm{hh}} & M_{\mathrm{vh}} \\ M_{\mathrm{hv}} & M_{\mathrm{vv}} \end{bmatrix} \\ &= A(r,\theta)e^{j\varphi} \begin{bmatrix} 1 & \delta_2 \\ \delta_1 & f_1 \end{bmatrix} \begin{bmatrix} \cos\Omega & \sin\Omega \\ -\sin\Omega & \cos\Omega \end{bmatrix} \begin{bmatrix} S_{\mathrm{hh}} & S_{\mathrm{vh}} \\ S_{\mathrm{hv}} & S_{\mathrm{vv}} \end{bmatrix} \\ &\quad \times \begin{bmatrix} \cos\Omega & \sin\Omega \\ -\sin\Omega & \cos\Omega \end{bmatrix} \begin{bmatrix} 1 & \delta_3 \\ \delta_4 & f_2 \end{bmatrix} + \begin{bmatrix} N_{\mathrm{hh}} & N_{\mathrm{vh}} \\ N_{\mathrm{hv}} & N_{\mathrm{vv}} \end{bmatrix} \end{aligned} \tag{2}$$

where S_{hh}, S_{hv}, S_{vh}, and S_{vv} are the components of the true scattering matrix, Ω is the Faraday rotation angle, f_1 and f_2 are the channel imbalance terms, δ_i, $i = 1$–4, are the crosstalk terms, and N_{pq} are the noise terms. Note that notations S_{pq} and M_{pq} indicate the scattering into channel q from a received signal in channel p, whereas several studies use the opposite (e.g., see [12]).

Equation (2) can be written as

$$\mathbf{M} = A(r,\theta)e^{j\varphi}\mathbf{GFS} + \mathbf{N} \tag{3}$$

where

$$\mathbf{G} = \begin{bmatrix} 1 & \delta_2 & \delta_4 & \delta_2\delta_4 \\ \delta_1 & f_1 & \delta_1\delta_4 & f_1\delta_4 \\ \delta_3 & \delta_2\delta_3 & f_2 & f_2\delta_2 \\ \delta_1\delta_3 & f_1\delta_3 & f_2\delta_1 & f_1 f_2 \end{bmatrix} \tag{4a}$$

$$\mathbf{F} = \begin{bmatrix} c^2 & cs & -cs & -s^2 \\ -cs & c^2 & s^2 & -cs \\ cs & s^2 & c^2 & cs \\ -s^2 & cs & -cs & c^2 \end{bmatrix}. \tag{4b}$$

Here, the measured and true scattering vectors are $\mathbf{M} = [M_{\mathrm{hh}}, M_{\mathrm{hv}}, M_{\mathrm{vh}}, M_{\mathrm{vv}}]^T$ and $\mathbf{S} = [S_{\mathrm{hh}}, S_{\mathrm{hv}}, S_{\mathrm{vh}}, S_{\mathrm{vv}}]^T$, respectively, $\mathbf{N} = [N_{\mathrm{hh}}, N_{\mathrm{hv}}, N_{\mathrm{vh}}, N_{\mathrm{vv}}]^T$ is an additive noise vector, $c = \cos\Omega$, and $s = \sin\Omega$. This paper does not deal with absolute calibration; thus, in the following, we omit the scalar term, i.e., $A(r,\theta)e^{j\phi}$. In addition, we will write f_i as $f_i = 1 + \varepsilon_i$, where ε_i is expected to be small; this assumes that the channel imbalance has been corrected for any significant nonzero mean phase, which is a standard step before level-1A processing, but there might be a small residual unknown phase offset.

If the system matrix, i.e., $\mathbf{G}$, is known, the system distortion can be removed by multiplying (3) by $\mathbf{G}^{-1}$ to give

$$\mathbf{G^{-1}M} = \mathbf{FS} + \mathbf{G^{-1}N}. \tag{5}$$

However, in practice, $\mathbf{G}$ and its inverse will not be exactly known either because the radar is engineered well enough that correction for the system distortion is considered unnecessary or because $\mathbf{G}$ has been estimated to yield a matrix $\hat{\mathbf{G}}$. Methods to derive $\hat{\mathbf{G}}$ using instrumented calibration sites (which normally require the effects of the Faraday rotation to be accounted for) are described in [17] and [19]–[23], but for positions close enough to the magnetic equator, the Faraday rotation can be neglected, and methods based on either instrumented sites or distributed targets can be used [24]–[26].

A more realistic form of (5) is therefore

$$\hat{\mathbf{G}}^{-1}\mathbf{M} = \hat{\mathbf{G}}^{-1}\mathbf{GFS} + \hat{\mathbf{G}}^{-1}\mathbf{N}. \tag{6}$$

This also covers the case where no correction is applied, in which case $\hat{\mathbf{G}}$ is replaced by the identity matrix. It is shown in [18] that to first order (6) can be written as

$$\hat{\mathbf{M}} = \hat{\mathbf{G}}^{-1}\mathbf{M} = \mathbf{FS} + (\mathbf{E}_1 + \mathbf{E}_2)\mathbf{FS} + \mathbf{N}' \tag{7}$$

where $\mathbf{N}' = \hat{\mathbf{G}}^{-1}\mathbf{N}$, and $\mathbf{E}_1$ and $\mathbf{E}_2$ are matrices only containing crosstalk and channel imbalance terms as follows:

$$\mathbf{E}_1 = \begin{bmatrix} 0 & \Delta\delta_2 & \Delta\delta_4 & 0 \\ \Delta\delta_1 & 0 & 0 & \Delta\delta_4 \\ \Delta\delta_3 & 0 & 0 & \Delta\delta_2 \\ 0 & \Delta\delta_3 & \Delta\delta_1 & 0 \end{bmatrix}$$

$$\mathbf{E}_2 = \begin{bmatrix} 0 & 0 & 0 & 0 \\ 0 & \Delta\varepsilon_1 & 0 & 0 \\ 0 & 0 & \Delta\varepsilon_2 & 0 \\ 0 & 0 & 0 & \Delta\varepsilon_1 + \Delta\varepsilon_2 \end{bmatrix}.$$

Here, $\Delta\delta_i = \delta_i - \hat{\delta}_i$, and $\Delta\varepsilon_i = \varepsilon_i - \hat{\varepsilon}_i$, where $\hat{\delta}_i$ and $\hat{\varepsilon}_i$ are the estimates of δ_i and ε_i, respectively, if calibration is performed, or they are zero if not. If the data are uncalibrated, $\Delta\delta_i$ and $\Delta\varepsilon_i$ should be replaced by δ_i and ε_i, respectively, in these and all subsequent expressions.

The terms on the right-hand side of (7) can be expanded as

$$\mathbf{FS} = \begin{pmatrix} c^2 S_{\rm hh} - s^2 S_{\rm vv} \\ -cs\,(S_{\rm hh} + S_{\rm vv}) + S_{\rm hv} \\ cs\,(S_{\rm hh} + S_{\rm vv}) + S_{\rm hv} \\ -s^2 S_{\rm hh} + c^2 S_{\rm vv} \end{pmatrix} \tag{8a}$$

$$\mathbf{E_1 FS} = \begin{pmatrix} \Delta\delta_2[FS]_2 + \Delta\delta_4[FS]_3 \\ \Delta\delta_1[FS]_1 + \Delta\delta_4[FS]_4 \\ \Delta\delta_3[FS]_1 + \Delta\delta_2[FS]_4 \\ \Delta\delta_3[FS]_2 + \Delta\delta_1[FS]_3 \end{pmatrix} \tag{8b}$$

$$\mathbf{E_2 FS} = \begin{pmatrix} 0 \\ \Delta\varepsilon_1[FS]_2 \\ \Delta\varepsilon_2[FS]_3 \\ (\Delta\varepsilon_1 + \Delta\varepsilon_2)[FS]_4 \end{pmatrix} \tag{8c}$$

where $[FS]_i$ denotes the ith component in the 4×1 vector $\mathbf{FS}$.

III. Effect of Distortion Uncertainties on Estimates of Faraday Rotation

Here, we analyze the accuracy with which the Faraday rotation can be estimated using the algorithm in [5] under the first-order approximations in (7) and (8). When the system distortion and noise are neglected, we can set

$$A = M_{\rm hh} + M_{\rm vv} = (S_{\rm hh} + S_{\rm vv})\cos 2\Omega \tag{9a}$$

$$B = M_{\rm vh} - M_{\rm hv} = (S_{\rm hh} + S_{\rm vv})\sin 2\Omega. \tag{9b}$$

Defining

$$Z_1 = A + jB = (S_{\rm hh} + S_{\rm vv})e^{2j\Omega} \tag{10a}$$

$$Z_2 = A - jB = (S_{\rm hh} + S_{\rm vv})e^{-2j\Omega} \tag{10b}$$

an estimator for Ω is given by [5]

$$\hat{\Omega} = \frac{1}{4}\arg\left(Z_1 Z_2^*\right). \tag{11a}$$

More generally, since the covariance term in (11a) is subject to large statistical fluctuations, a good estimate of Ω requires taking the expected value, which is denoted by $\langle\cdot\rangle$, so that

$$\hat{\Omega} = \frac{1}{4}\arg\left\langle Z_1 Z_2^*\right\rangle. \tag{11b}$$

In practice, this is approximated by averaging over many pixels (or looks), and somewhat imprecisely, we use the same notation for the average.

When the system distortion and noise are present, the expressions in (9) become modified to

$$\hat{A} = A + \Delta A = (S_{\rm hh} + S_{\rm vv})\cos 2\Omega + A_1 + A_2 + \mathbf{N'}_{\rm hh} + \mathbf{N'}_{\rm vv} \tag{12a}$$

$$\hat{B} = B + \Delta B = (S_{\rm hh} + S_{\rm vv})\sin 2\Omega + B_1 + B_2 + \mathbf{N'}_{\rm vh} - \mathbf{N'}_{\rm hv} \tag{12b}$$

where

$$A_1 = S_{\rm hv}(\Delta\delta_1 + \Delta\delta_2 + \Delta\delta_3 + \Delta\delta_4) + cs(S_{\rm hh} + S_{\rm vv})(\Delta\delta_1 - \Delta\delta_3 + \Delta\delta_4 - \Delta\delta_2) \tag{13a}$$

$$B_1 = S_{\rm hh}(c^2[\Delta\delta_3 - \Delta\delta_1] - s^2[\Delta\delta_2 - \Delta\delta_4]) + S_{\rm vv}(c^2[\Delta\delta_2 - \Delta\delta_4] - s^2[\Delta\delta_3 - \Delta\delta_1]) \tag{13b}$$

$$A_2 = (\Delta\varepsilon_1 + \Delta\varepsilon_2)(-s^2 S_{\rm hh} + c^2 S_{\rm vv}) \tag{13c}$$

$$B_2 = S_{\rm hv}(\Delta\varepsilon_2 - \Delta\varepsilon_1) + cs(S_{\rm hh} + S_{\rm vv})(\Delta\varepsilon_2 + \Delta\varepsilon_1) \tag{13d}$$

and the N'_{pq} terms come from the noise vector $\hat{\mathbf{G}}^{-1}\mathbf{N}$ in (7).

Set

$$X_{31} = \Delta\delta_3 - \Delta\delta_1 = P + jQ \tag{14a}$$

$$X_{24} = \Delta\delta_2 - \Delta\delta_4 = U + jV \tag{14b}$$

$$\Sigma_\delta = \Delta\delta_1 + \Delta\delta_3 + \Delta\delta_2 + \Delta\delta_4 \tag{14c}$$

$$Y_{21} = \Delta\varepsilon_2 - \Delta\varepsilon_1 \tag{14d}$$

$$\Sigma_\varepsilon = \Delta\varepsilon_2 + \Delta\varepsilon_1 = C + jD. \tag{14e}$$

Here, X_{31} is the difference between the corrected crosstalk from V into H on transmit and the corrected crosstalk from H into V on receive, whereas X_{24} is the difference between the corrected crosstalk from V into H on receive and the corrected crosstalk from H into V on transmit. An involved calculation (see the Appendix) then yields

$$\begin{aligned} \left\langle \hat{Z}_1 \hat{Z}_2^* \right\rangle &\approx \left\langle (\hat{A} + j\hat{B})(\hat{A} - j\hat{B})^* \right\rangle \\ &\approx e^{4j\Omega}\left(\left\langle |S_{hh} + S_{vv}|^2 \right\rangle + 2R\cos\theta(jP + jU + C)\right) \\ &\quad + 2e^{3j\Omega}\left(P(jc\sigma_{hh} - s\sigma_{vv}) + U(-s\sigma_{hh} + jc\sigma_{vv})\right. \\ &\quad \left. + C(js\sigma_{hh} + c\sigma_{vv})\right) + 2e^{2j\Omega}R\sin\theta \\ &\quad \times (-jQ + jV + D) + 2e^{2j\Omega} \\ &\quad \times \langle \mathrm{Re}\left((S_{hh} + S_{vv})\, S_{hv}^* \Sigma_\delta^*\right) \\ &\quad + j\mathrm{Re}\left((S_{hh} + S_{vv})\, S_{hv}^* Y_{21}^*\right)\rangle. \end{aligned} \tag{15}$$

where the copolarized backscattering coefficients are written as

$$\sigma_{pp} = \left\langle |S_{\rm pp}|^2 \right\rangle$$

and the HH–VV covariance is given by

$$R{\rm e}^{j\theta} = \langle S_{\rm hh} S_{\rm vv}^* \rangle \, .$$

Here, we have assumed that there is no correlation between the signal and the noise or between the noise in each channel and that the noise powers are the same in all channels. Hence, the noise does not lead to bias, although it will cause higher variability in regions where the signal-to-noise ratio is smaller. However, if the sum of the noise powers in the copolarized channels is different from the sum in the cross-polarized channels, some noise bias will remain (see the Appendix).

The argument of the left-hand side of (15) is, by definition, $4\hat{\Omega}$; thus, we can write

$$\begin{aligned}\left\langle \left| \hat{Z}_1^* \hat{Z}_2 \right| \cos 4\hat{\Omega} \right\rangle = & \left\langle |S_{\rm hh} + S_{\rm vv}|^2 \right\rangle \cos 4\Omega \\ & - 2(Pc\sigma_{\rm hh} + Uc\sigma_{\rm vv} + Cs\sigma_{\rm hh}) \sin 3\Omega \\ & - 2(Ps\sigma_{\rm vv} + Us\sigma_{\rm hh} - Cc\sigma_{\rm vv}) \cos 3\Omega \\ & + 2R\cos\theta\,(-(P+U)\sin 4\Omega + C\cos 4\Omega) \\ & + 2R\sin\theta\,(-(V-Q)\sin 2\Omega + D\cos 2\Omega) \\ & + 2\cos 2\Omega\,\langle {\rm Re}\,((S_{\rm hh} + S_{\rm vv})\, S_{\rm hv}^* \Sigma_\delta^*)\rangle \\ & - 2\sin 2\Omega\,\langle {\rm Re}\,((S_{\rm hh} + S_{\rm vv})\, S_{\rm hv}^* Y_{21}^*)\rangle \end{aligned} \tag{16a}$$

$$\begin{aligned}\left\langle \left| \hat{Z}_1^* \hat{Z}_2 \right| \sin 4\hat{\Omega} \right\rangle = & \left\langle |S_{\rm hh} + S_{\rm vv}|^2 \right\rangle \sin 4\Omega \\ & + 2(Pc\sigma_{\rm hh} + Uc\sigma_{\rm vv} + Cs\sigma_{\rm hh}) \cos 3\Omega \\ & + 2(-Ps\sigma_{\rm vv} - Us\sigma_{\rm hh} + Cc\sigma_{\rm vv}) \sin 3\Omega \\ & + 2R\cos\theta\,((P+U)\cos 4\Omega + C\sin 4\Omega) \\ & + 2R\sin\theta\,((V-Q)\cos 2\Omega + D\sin 2\Omega) \\ & + 2\sin 2\Omega\,\langle {\rm Re}\,((S_{\rm hh} + S_{\rm vv})\, S_{\rm hv}^* \Sigma_\delta^*)\rangle \\ & + 2\cos 2\Omega\,\langle {\rm Re}\,((S_{\rm hh} + S_{\rm vv})\, S_{\rm hv}^* Y_{21}^*)\rangle \, . \end{aligned} \tag{16b}$$

In the Appendix, (16) is used to derive the first-order form for $\tan(4\hat{\Omega} - 4\Omega)$ shown at the bottom of the page, where quantities T and W are target dependent as follows:

$$T = \frac{\sigma_{\rm hh} - \sigma_{\rm vv} + 2jR\sin\theta}{\sigma_{\rm hh} + \sigma_{\rm vv} + 2R\cos\theta} \tag{18a}$$

$$W = \frac{\langle (S_{\rm hh} + S_{\rm vv})\, S_{\rm hv}^* \rangle}{\left\langle |S_{\rm hh} + S_{\rm vv}|^2 \right\rangle}. \tag{18b}$$

Hence, the bias only depends on ${\rm Re}(X_{31} + X_{24})$, $X_{31} - X_{24}$, Σ_ε, T, and W. Note that (17) simplifies under reflection symmetry since $\langle S_{\rm hh} S_{\rm hv}^* \rangle = \langle S_{\rm vv} S_{\rm hv}^* \rangle = 0$, $W = 0$, and the last terms in the numerator and the denominator vanish. Note also that the presence of system distortion means that the measured Faraday rotation is no longer decoupled from the target properties, unlike in the ideal case [the first term in (15)].

TABLE I
(a) COVARIANCE MATRIX VALUES FOR DIFFERENT BIOMASS VALUES AND (b) ASSOCIATED VALUES OF T, t, τ, AND THE MAXIMUM BIAS IN Ω WHEN $\Omega = 0°$ DERIVED FROM THE FIRST-ORDER APPROXIMATION (30) WHEN THE DISTORTION AMPLITUDES DO NOT EXCEED (a) 0.1 (−20 dB) AND (b) 0.0316 (−30 dB)

Biomass (t ha^{-1})	σ_{hh} (m^2/m^2)	σ_{vv} (m^2/m^2)	σ_{hv} (m^2/m^2)	R	θ (degs.)
50	0.213	0.250	0.040	0.086	-54.6
200	0.649	0.274	0.073	0.150	-96.8
350	1.018	0.281	0.092	0.172	-139.1

(a)

Biomass (t ha^{-1})	T	t	τ(degs.)	$\hat{\Omega} - \Omega$ (degs) Distortion amps< 0.1 (left); 0.0316 (right)
50	-0.0665-0.2483j	0.2571	-105.0	7.0; 2.0
200	0.4223-0.3363j	0.5439	-38.5	6.6; 2.0
350	0.7087-0.2164j	0.7410	-17.0	6.1; 1.9

(b)

Although the focus of this paper is on the bias in the estimated Faraday rotation derived from (17), it should be noted that the overall error includes a random component arising from the noise and the fact that (11b) uses an estimated covariance term, which is subject to an uncertainty that decreases as the number of looks increases [15]. This does not form part of our analysis but can be investigated using simulation, as discussed in Section IV.

The single-look form of T can be written as

$$\frac{S_{\rm hh} - S_{\rm vv}}{S_{\rm hh} + S_{\rm vv}}$$

but this is not applicable since averaging is needed to estimate Ω with reasonable accuracy. Note also that $|T|$ can, in principle, range from 0 to ∞ since, if $\theta = \pi$ and R takes its maximum possible value $\sqrt{\sigma_{\rm hh}\sigma_{\rm vv}}$, we have

$$\begin{aligned} |T| &= \frac{|\sigma_{\rm hh} - \sigma_{\rm vv}|}{\sigma_{\rm hh} + \sigma_{\rm vv} - 2\sqrt{\sigma_{\rm hh}\sigma_{\rm vv}}} \\ &= \frac{\left|\left(\sqrt{\sigma_{\rm hh}} + \sqrt{\sigma_{\rm vv}}\right)\left(\sqrt{\sigma_{\rm hh}} - \sqrt{\sigma_{\rm vv}}\right)\right|}{\left(\sqrt{\sigma_{\rm hh}} - \sqrt{\sigma_{\rm vv}}\right)^2} \\ &= \left| \frac{\sqrt{\sigma_{\rm hh}} + \sqrt{\sigma_{\rm vv}}}{\sqrt{\sigma_{\rm hh}} - \sqrt{\sigma_{\rm vv}}} \right| \end{aligned}$$

which tends to ∞ as $\sigma_{\rm vv} \to \sigma_{\rm hh}$. However, in the calculations in Section V, which are based on measurements from boreal forest for different levels of biomass, $0.25 < |T| < 0.75$ [see Table I(b)].

$$E = \tan(4\hat{\Omega} - 4\Omega) = \frac{{\rm Re}\left\{X_{31} + X_{24} + T\left(\Sigma_\varepsilon \sin 2\Omega + (X_{31} - X_{24})\cos 2\Omega\right) + 2W(-\Sigma_\delta^* \sin 2\Omega + Y_{21}^* \cos 2\Omega)\right\}}{1 + {\rm Re}\left\{\Sigma_\varepsilon + T\left(-\Sigma_\varepsilon \cos 2\Omega + (X_{31} - X_{24})\sin 2\Omega\right) + 2W(\Sigma_\delta^* \cos 2\Omega + Y_{21}^* \sin 2\Omega)\right\}} \tag{17}$$

A. Maximizing Bias in Ω

Equation (17) can be used to find the largest possible bias in Ω and the properties of the distortion terms that give rise to it since this is equivalent to finding the maximum absolute value of $\tan(4\hat{\Omega} - 4\Omega)$. However, this becomes complicated in the general case; thus, here, we only perform the analysis for azimuthally symmetric targets, i.e., we set $W = 0$ in (17). All references to (17) in the following assume this simplified form.

To carry out the optimization, we set

$$\begin{aligned} X_{31} &= ue^{j\phi_3} \\ X_{24} &= ve^{j\phi_2} \\ \Sigma_\varepsilon &\equiv pe^{j\psi} \\ T &\equiv te^{j\tau} \\ \tilde{C} &= \cos 2\Omega \\ \tilde{S} &= \sin 2\Omega. \end{aligned} \tag{19}$$

The reason for indexing the angles in X_{31} and X_{24} as 3 and 2, respectively, will become clear in the following. We can then write

$$E = \frac{N}{D} \tag{20a}$$

where

$$\begin{aligned} N &= u\cos\phi_3 + v\cos\phi_2 + \text{Re}\left\{\tilde{S}T\Sigma_\varepsilon + \tilde{C}T\left(ue^{j\phi_3} - ve^{j\phi_2}\right)\right\} \\ &= u\cos\phi_3 + v\cos\phi_2 + \tilde{S}pt\cos[\tau+\psi] \\ &\quad + \tilde{C}t\left\{u\cos[\tau+\phi_3] - v\cos[\tau+\phi_2]\right\} \end{aligned} \tag{20b}$$

$$\begin{aligned} D &= 1 + \text{Re}(\Sigma_\varepsilon) - \tilde{C}\text{Re}(T\Sigma_\varepsilon) + \tilde{S}\text{Re}\left\{T\left(ue^{j\phi_3} - ve^{j\phi_2}\right)\right\} \\ &= 1 + p\cos\psi - \tilde{C}pt\cos[\tau+\psi] \\ &\quad + \tilde{S}t\left\{u\cos[\tau+\phi_3] - v\cos[\tau+\phi_2]\right\} \end{aligned} \tag{20c}$$

are the numerator and the denominator in (17), respectively. Hence

$$\begin{aligned} \frac{\partial E}{\partial u} &= \frac{\left(\cos\phi_3 + \tilde{C}t\cos[\tau+\phi_3]\right)D - \tilde{S}t\cos[\tau+\phi_3]N}{D^2} \\ &= \frac{D\cos\phi_3 + t\cos[\tau+\phi_3](\tilde{C}D - \tilde{S}N)}{D^2}. \end{aligned} \tag{21a}$$

Similarly

$$\frac{\partial E}{\partial v} = \frac{D\cos\phi_2 - t\cos[\tau+\phi_2](\tilde{C}D - \tilde{S}N)}{D^2}. \tag{21b}$$

Set $K = \tilde{S}pt\cos[\tau+\psi]$ and $L = 1 + p\cos\psi - \tilde{C}pt\cos[\tau+\psi]$; thus, K and L are independent of u, v, and ϕ_i. Then, $\tilde{C}D - \tilde{S}N = \tilde{C}L - \tilde{S}(u\cos\phi_3 + v\cos\phi_2 + K)$, and we can write the numerator of (21a) as

$$\begin{aligned} &t\cos[\tau+\phi_3]\left\{\tilde{C}L - \tilde{S}\left(v\cos\phi_2 + K\right)\right\} \\ &\quad + \cos\phi_3\left\{L - \tilde{S}tv\cos[\tau+\phi_2]\right\}. \end{aligned} \tag{22a}$$

Hence, the sign of $\partial E/\partial u$ is independent of u; thus, E is monotonic in u. Similarly, the numerator of (21b) is

$$\begin{aligned} &-t\cos[\tau+\phi_2]\left\{\tilde{C}L - \tilde{S}\left(U\cos\phi_3 + K\right)\right\} \\ &\quad + \cos\phi_2\left\{L + \tilde{S}tu\cos[\tau+\phi_3]\right\} \end{aligned} \tag{22b}$$

so that E is monotonic in v. Similar analysis also applies to p in (17). Hence, the bias in the Faraday rotation will have its maximum modulus when each of u, v, and p attains its maximum value.

The maximum values of u, v, and p can be readily related to the values of $\Delta\delta_i$ and $\Delta\varepsilon_i$. For given values of $|\Delta\delta_1|$ and $|\Delta\delta_3|$, u will be maximized when $\Delta\delta_1$ and $\Delta\delta_3$ have opposite signs, i.e., their arguments are π out of phase. If $|\Delta\delta_1|$ and $|\Delta\delta_3|$ have the same value, then $\Delta\delta_1 = -\Delta\delta_3$, $X_{31} = 2\Delta\delta_3$, and $\arg(\Delta\delta_3) = \arg(X_{31}) = \phi_3$. Similarly, $\Delta\delta_4 = -\Delta\delta_2$, $X_{24} = 2\Delta\delta_2$, and $\arg(\Delta\delta_2) = \arg(X_{24}) = \phi_2$ (hence the choice of the indexing for the angles). For the maximum Faraday rotation bias, the amplitudes of $\Delta\delta_i$ should be as large as possible, and if they all have the same upper bound, i.e., $\Delta\delta_M$, then $u = v = 2\Delta\delta_M$. Similarly, if the channel imbalance terms have the same upper bound, i.e., $\Delta\varepsilon_M$, the maximum value of p occurs when $\Delta\varepsilon_1 = \Delta\varepsilon_2$ and $|\Delta\varepsilon_1| = \Delta\varepsilon_M$; thus, $p = 2\Delta\varepsilon_M$, and $\arg(\Delta\varepsilon_1) = \psi$. Hence, for the maximum Faraday rotation bias, X_{31}, X_{24}, and Σ_ε should be replaced by $2\Delta\delta_M e^{j\phi_3}$, $2\Delta\delta_M e^{j\phi_2}$, and $2\Delta\varepsilon_M e^{j\psi}$, respectively, in (17).

A relation between the phases of the crosstalk terms giving the maximum bias can be derived by differentiating (17) as follows:

$$\frac{\partial E}{\partial\phi_3} = \frac{-\left(u\sin\phi_1 + \tilde{C}tu\sin[\tau+\phi_3]\right)D + \tilde{S}tu\sin[\tau+\phi_3]N}{D^2}$$

so that

$$\frac{D^2}{u}\frac{\partial E}{\partial\phi_3} = -\sin\phi_3 D - (\tilde{C}D - \tilde{S}N)t\sin[\tau+\phi_3]. \tag{23a}$$

Similarly

$$\frac{D^2}{v}\frac{\partial E}{\partial\phi_2} = -\sin\phi_2 D + (\tilde{C}D - \tilde{S}N)t\sin[\tau+\phi_2]. \tag{23b}$$

For the maximum Faraday rotation bias, both these expressions should be set to 0. Multiplying (23a) by $\sin\phi_2$ and (23b) by $\sin\phi_3$ and subtracting leads to the following relation:

$$\sin\phi_2\sin(\tau+\phi_3) + \sin\phi_3\sin(\tau+\phi_2) = 0$$

which is equivalent to

$$2\cos(\tau+\phi_3+\phi_2) - \cos(\tau-\phi_3+\phi_2) - \cos(\tau+\phi_3-\phi_2) = 0$$

or

$$\cos(\tau+\phi_3+\phi_2) - \cos\tau\cos(\phi_3-\phi_2) = 0.$$

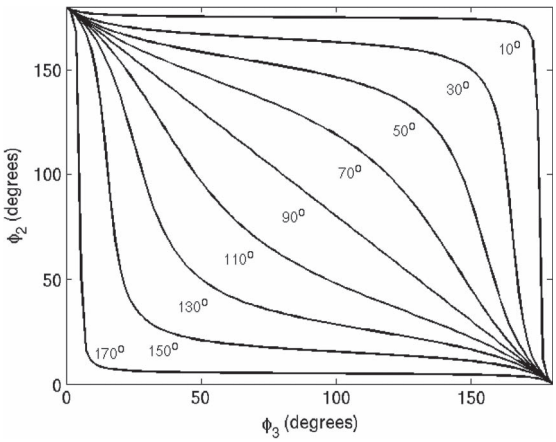

Fig. 1. Relationship between angles ϕ_2 and ϕ_3 giving the maximum Faraday rotation estimation bias for the values of τ indicated on each curve.

Hence

$$-2\cot\tau = \cot\phi_2 + \cot\phi_3. \tag{24}$$

The plot of (24) for fixed values of τ in Fig. 1 shows that, when τ is close to 0° or 180°, ϕ_2 or ϕ_3 must be close to zero for the bias to be a maximum, whereas when τ is close to 90°, the maximum bias occurs when $\phi_2 + \phi_3 = 180^\circ$. Note that the phase relation (24) does not depend on Ω, but substituting it back into (23a) and (23b) and setting both to zero yields equations that depend on both Ω and the channel imbalance terms.

B. Bias in Faraday Rotation Estimate When $\Omega = 0$

For a general value of Ω, an analytic approach to maximizing (17) is complicated but can be readily developed if $\Omega = 0$, which, as explained in Section I, is important for both P-band and L-band. As shown in Section III-A, the maximal bias in Ω requires $|X_{31}| = |X_{24}| = 2\Delta\delta_M$ and $|\Sigma_\varepsilon| = 2\Delta\varepsilon_M$, assuming all the crosstalk terms are constrained to have maximum amplitude $\Delta\delta_M$ and the channel imbalance terms have maximum amplitude $\Delta\varepsilon_M$. Hence, when $\Omega = 0$, (17) becomes

$$E = 2\Delta\delta_M \frac{\cos\phi_3 + \cos\phi_2 + t\{\cos[\tau+\phi_3] - \cos[\tau+\phi_2]\}}{1 + 2\Delta\varepsilon_M\{\cos\psi - t\cos[\tau+\psi]\}}. \tag{25}$$

The terms in ψ can be written as

$$\cos\psi(1 - t\cos\tau) + t\sin\psi\sin\tau \equiv R_1\sin(\psi+\alpha_1) \tag{26a}$$

where

$$R_1^2 = (1-t\cos\tau)^2 + (t\sin\tau)^2 = 1 + t^2 - 2t\cos\tau = |1-T|^2 \tag{26b}$$

$$\tan\alpha_1 = \frac{1-t\cos\tau}{t\sin\tau}. \tag{26c}$$

Similarly, we can write

$$\cos\phi_2(1 - t\cos\tau) + t\sin\phi_2\sin\tau \equiv R_2\sin(\phi_2+\alpha_2) \tag{27}$$

where $R_2 = R_1$, and $\alpha_2 = \alpha_1$, and

$$\cos\phi_3(1+t\cos\tau) - t\sin\phi_3\sin\tau \equiv R_3\cos(\phi_3+\alpha_3) \tag{28a}$$

where

$$R_3^2 = 1 + t^2 + 2t\cos\tau = |1+T|^2 \tag{28b}$$

$$\tan\alpha_3 = \frac{t\sin\tau}{1+t\cos\tau}. \tag{28c}$$

Hence

$$E = 2\Delta\delta_M \frac{|1+T|\cos(\phi_3+\alpha_3) + |1-T|\sin(\phi_2+\alpha_2)}{1 + 2\Delta\varepsilon_M|1-T|\sin(\psi+\alpha_2)}. \tag{29}$$

This will be maximized by making the numerator as large as possible and the denominator as small as possible, which clearly implies setting $\phi_3 = -\alpha_3$, $\phi_2 = \pi/2 - \alpha_2$, and $\psi = -\pi/2 - \alpha_2$. Hence, the maximal bias in $\tan(4\hat{\Omega} - 4\Omega)$ is

$$E = 2\Delta\delta_M \frac{|1+T| + |1-T|}{1 - 2\Delta\varepsilon_M|1-T|}. \tag{30}$$

This occurs when $\Delta\delta_3 = -\Delta\delta_1 = \Delta\delta_M e^{-j\alpha_3}$, $\Delta\delta_2 = -\Delta\delta_4 = j\Delta\delta_M e^{-j\alpha_1}$, and $\Delta\varepsilon_1 = \Delta\varepsilon_2 = -j\Delta\varepsilon_M e^{-j\alpha_1}$; thus, $\arg(\Delta\varepsilon_1) = \arg(\Delta\varepsilon_2) = \arg(\Delta\delta_4)$, where α_1 and α_3 are given by (26c) and (28c), respectively.

This analysis makes clear that the Faraday rotation bias depends not just on the amplitudes of the distortion terms but also on their relative phases and the relation between these phases and the phase of the HH–VV covariance in the target region. Hence, the bias will vary with position in a scene.

IV. Exact Simulations

To test the accuracy of the first-order approximations derived in Sections II and III, we developed a simulator for the measurement process that makes no approximations and directly works from the system model (2). The simulator also contains modules that allow the system distortion terms to be estimated from a set of point target measurements by a range of algorithms, e.g., see [16]. These estimates can then be applied to carry out the calibration procedure in (6). However, in the simulations in this paper, no calibration is performed, and the errors in the estimates arise purely from uncorrected system distortions and noise.

In order to define the values of T and W in (17), the simulation procedure needs as input a covariance matrix characterizing the cover type where the measurement is being made. Here, we take advantage of the BIOMASS End-to-End Mission Performance Simulator (BEES) [27], which is able to provide the P-band covariance matrices of forest regions as a function of their biomass density based on airborne measurements. In this paper, we use the values from BEES appropriate to a boreal forest, the underlying data of which were taken during the 2007 BIOSAR-1 campaign in Sweden [28]. A range of biomass values is considered that gives a wide variation in covariance properties (see Table I), from similar copolarized backscattering coefficients for a lower biomass to a factor five difference between them for a high biomass, with copolarized phase

differences varying by nearly 90°. (Note that the simulated covariance for a biomass of 350 t · ha^{-1} is outside the observed range but is included here because the increased dominance of the double-bounce scattering simulated by BEES produces large HH/VV ratios and large copolar phase differences.) This allows the sensitivity of the Faraday rotation errors to variation in the cover type to be explored in a way that is not specific to forest regions. It also means that, in the calculations, "biomass" is effectively just a way of labeling different covariance matrices and is not in itself a relevant variable.

Although it would, in principle, be feasible to do so, the simulations carried out in this paper do not account for distortions in the polarimetric covariance matrix caused by topographic variation (particularly azimuth slopes [29]) and assume azimuth symmetry (i.e., $W = 0$) with no correlation between the copolarized and cross-polarized channels. This is for practical reasons, i.e., representing topography would involve the simulation of different topographic conditions in addition to variability in the distortion terms, which would greatly increase the computation necessary in order to derive statistically valid conclusions.

The simulation involves four steps as follows.

1) *Scene data generation*. For biomass value B, we generate a large set of independent scattering matrix realizations from a zero-mean Gaussian distribution with covariance matrix $C(B)$ using Choleski decomposition. Hence, the data are exactly characterized and can be used to test the validity of the first-order theory without complications introduced by interpixel correlation, point-spread function effects, etc. However, the simulator can readily accept data from other sources, such as real data or the output from BEES [27].
2) *Data distortion*. The data are corrupted with system distortion, Faraday rotation, and noise, as in (2). Typically, a set of equally spaced values of Ω in the range $-\pi < \Omega < \pi$ is considered, and for each value of Ω, many random realizations of the distortion matrix are generated under constraints on the amplitude of the distortion terms. In all the simulations in Section V, the phases are taken to be uniformly distributed between $\pm\pi$.
3) *Estimation of the Faraday rotation*. Estimate Ω at each position using (11b).
4) *Derivation of measurement statistics and worst case estimates*. By performing Steps 1–3 for many realizations of the scene, the system distortion terms, the Faraday rotation, and the noise, we can derive histograms of the estimated distortion terms and Ω. This allows us to assess the accuracy of the first-order theory and to visualize how representative the worst case biases are.

Note that discrepancies between exact calculations and the first-order approximation can arise (see Section V-A) from both the approximation itself and the fact that the approximation uses exact values for the covariance terms. In contrast, the simulations use many realizations derived using the same covariance values (as described in Step 1) but are subject to statistical fluctuation. Hence, for example, the sample values of the co/cross-polarization covariance will not be identically zero.

V. Testing Predictions From First-Order Analysis

A comparison between the error $\hat{\Omega} - \Omega = (\tan^{-1} E)/4$ from (17) and that from the exact simulation is shown in Fig. 2(a) and (b) as a function of Ω for two random realizations of the distortion matrix, in which the amplitudes of all distortion terms are constrained not to exceed 0.1 (−20 dB) and the noise is neglected. The covariance values used in the calculations are for a biomass of 200 t · ha^{-1} [see Table I(a)]. Fig. 2(a) is typical, with the first-order approximation being very similar to the exact calculations, whereas Fig. 2(b) is an example of a less good match. The overall spread of errors is represented in Fig 2(c), which shows a histogram of the error in Ω using the exact calculations for 50 000 random realizations of the system distortion, where each realization was generated by sampling from uniform distributions over the ranges [0, δ_M] and [0, ε_M] for the amplitudes of δ_i and ε_i, respectively, whereas the phases of δ_i, ε_i, and Ω are uniformly distributed on [0, 2π]; each of these 13 variables is independently sampled. The error is unbiased and has a standard deviation of 1.3°. Over the same set of distortion values, the first-order approximation is also unbiased and has the same standard deviation. The difference between these two estimates, whose histogram is given in Fig. 2(d), is normally small, but for a small proportion of realizations, it can be as large as 0.5°. This suggests that, even for distortion amplitudes as large as 0.1, the first-order approximation is tenable. System noise up to NESZ $= -20$ dB has a negligible effect on either the bias or standard deviation of the error.

A. Maximum Bias in Faraday Rotation When $\Omega = 0$

The first-order estimates of the maximum possible Faraday rotation bias when $\Omega = 0$ for the covariance values corresponding to biomass values of 50, 200, and 350 t · ha^{-1} are given in Table I(b). These were calculated using (30), with the covariance values derived using BEES [27] [see Table I(a)]. The calculations use two values of this maximum distortion amplitude, i.e., 0.1 (−20 dB) and 0.0316 (−30 dB). The bias can exceed 6° for the −20 dB bound and 1.9° even for the −30 dB bound. As predicted, the maximum Faraday rotation bias varies, although not greatly, as the covariance properties of the target vary.

Table II gives the maximum Faraday rotation bias when $\Omega = 0$ derived from both (30) and the numerical optimization for the same three covariance matrices when the maximum permitted amplitude of the distortion terms is 0.1 (−20 dB) and 0.0316 (−30 dB), and when the noise is neglected. In addition, the phases of the crosstalk and channel imbalance terms giving rise to these maximal biases from both approaches are shown (in the optimization, the amplitudes of the distortion terms are all found to take their maximum possible values, as expected). The optimization was carried out as a constrained minimization problem using the negative of the square of the Faraday rotation error as the error function and with the amplitudes of the distortion terms constrained not to exceed the given values of $\Delta\delta_M$ and $\Delta\varepsilon_M$; the phases were unconstrained. (In fact, since

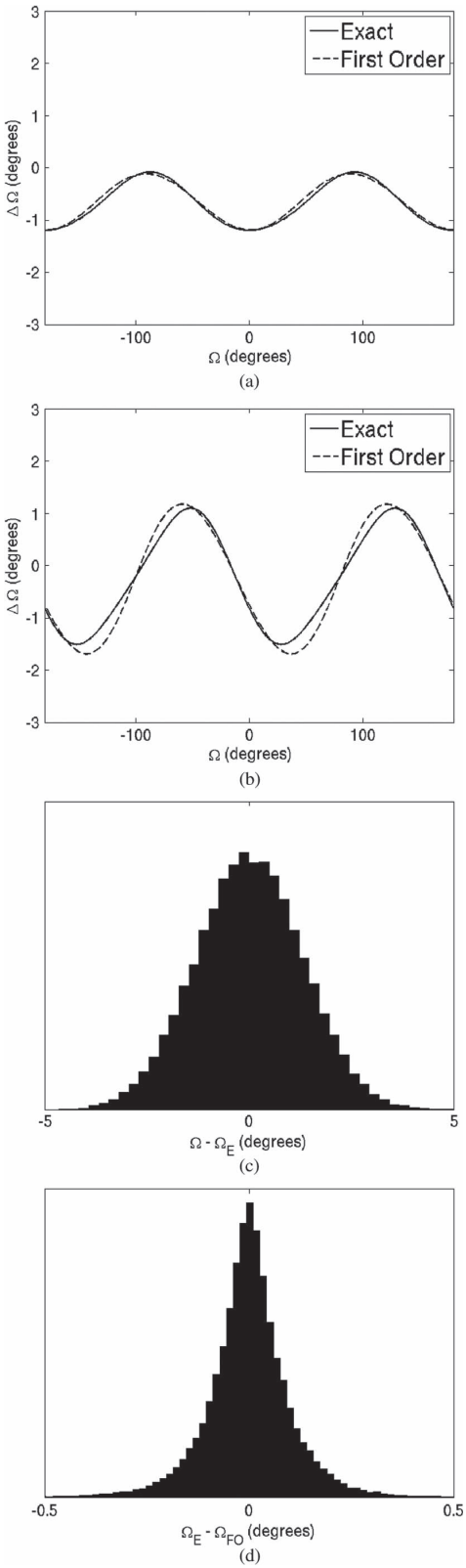

Fig. 2. (a) and (b) Comparison of the first-order approximation (dashed lines) and the simulated values (solid lines) of the error in Ω as a function of Ω for two random realizations of the system distortion with amplitudes < 0.1. (c) Histogram of the error in Ω using the exact simulation, i.e., Ω_E, for 50 000 random realizations of the system distortion, with amplitudes < 0.1 and values of Ω uniformly distributed between $\pm\pi$. (d) Histogram of the difference between the exact error in Ω and its first-order approximation, i.e., Ω_{FO}, corresponding to the data used in (c). The calculations are for a biomass of 200 t $\cdot$ ha^{-1} and neglect system noise.

TABLE II
MAXIMUM VALUE (IN DEGREES) OF THE FARADAY ROTATION BIAS FOR THREE LEVELS OF BIOMASS WHEN $\Omega = 0$ DERIVED FROM THE NUMERICAL OPTIMIZATION AND THE FIRST-ORDER APPROXIMATION (30) WHEN THE DISTORTION AMPLITUDES DO NOT EXCEED (a) 0.1 (-20 dB) AND (b) 0.0316 (-30 dB), AND WHEN THE SYSTEM NOISE IS NEGLECTED. AT THE MAXIMUM BIAS, THE DISTORTION TERMS ALL ASSUME THEIR MAXIMUM AMPLITUDE, WHEREAS THEIR PHASES ARE SHOWN IN THE TABLE

<-20dB		$\widehat{\Omega}-\Omega$	$\arg(\delta_1)$	$\arg(\delta_2)$	$\arg(\delta_3)$	$\arg(\delta_4)$	$\arg(\varepsilon_1)$	$\arg(\varepsilon_2)$
50 t/ha	optn	6.2	-166.6	-14.7	13.4	165.5	166.6	164.5
	1st order	7.0	-165.1	-13.1	14.9	166.9	166.9	166.9
200 t/ha	optn	6.3	-168.6	-35.2	11.1	143.6	154.1	177.1
	1st order	6.6	-166.7	-30.2	13.3	149.8	149.8	149.8
350 t/ha	optn	6.1	-173.0	-51.6	6.8	127.3	-157.7	-143.0
	1st order	6.1	-172.8	-36.6	7.2	143.4	143.4	143.4

(a)

<-30dB		$\widehat{\Omega}-\Omega$	$\arg(\delta_1)$	$\arg(\delta_2)$	$\arg(\delta_3)$	$\arg(\delta_4)$	$\arg(\varepsilon_1)$	$\arg(\varepsilon_2)$
50 t/ha	optn	1.9	-165.6	-13.1	14.4	166.5	170.2	164.9
	1st order	2.0	-165.1	-13.1	14.9	166.9	166.9	166.9
200 t/ha	optn	2.0	-167.2	-31.2	12.5	147.9	143.6	-164.3
	1st order	2.0	-166.7	-30.2	13.3	149.8	149.8	149.8
350 t/ha	optn	1.9	-172.9	-40.4	6.9	138.9	-166.8	-131.3
	1st order	1.9	-172.8	-36.6	7.2	143.4	143.4	143.4

(b)

the amplitudes always took their maximum possible values at the optima found by the algorithm, it could be treated as an unconstrained problem with the amplitudes fixed at their maxima.) A variety of algorithms were compared, all of which gave the same solutions, but the sequential quadratic programming algorithm [30] was found to be the quickest.

The predicted maximum bias agrees well with that found by the optimization, particularly when the distortion amplitudes are smaller. As predicted, the maximum bias occurs for $\arg(\delta_2) - \arg(\delta_1) = \arg(\delta_2) - \arg(\delta_4) = 180^\circ$ (thus, $\delta_3 = -\delta_1$, and $\delta_2 = -\delta_4$), and the phases of the crosstalk terms are also close to their predicted values, although with larger differences for the covariance matrices corresponding to the higher biomass values. However, the prediction that $\arg(\varepsilon_2) = \arg(\varepsilon_1) = \arg(\delta_4)$ is (approximately) satisfied only for the covariance matrix corresponding to a biomass of 50 t $\cdot$ ha^{-1}. The apparent discrepancies for the other covariance matrices can be traced to the fact that the sample co/cross covariances in the simulated data are small but nonzero. It can be shown that this changes the phase relations between the ε_i terms for which the maximum bias occurs but with only small effects on the size of the bias and on the δ_i terms. The closer approximation between the theory and the simulation for 50 t $\cdot$ ha^{-1} is because the sample co/cross covariance was particularly small in this case, simply as a result of statistical fluctuation in the simulated data.

To assess how representative the worst case biases are, the simulation was used to derive the histograms of the bias in Ω when $\Omega = 0$ for 50 000 random realizations of the system distortion, with amplitudes less than 0.1 and with no system noise [see Fig. 3(a)]. Similar calculations were also performed with all the distortion terms having a fixed amplitude of 0.1 [see Fig 3(b)]. The calculations are for a biomass of 200 t $\cdot$ ha^{-1}; thus, the maximum bias in both cases is 6.3° [see Table II(a)]. This bias occurs far out in the tail for both cases, but the corresponding cumulative density functions [see Fig. 3(c)] indicate

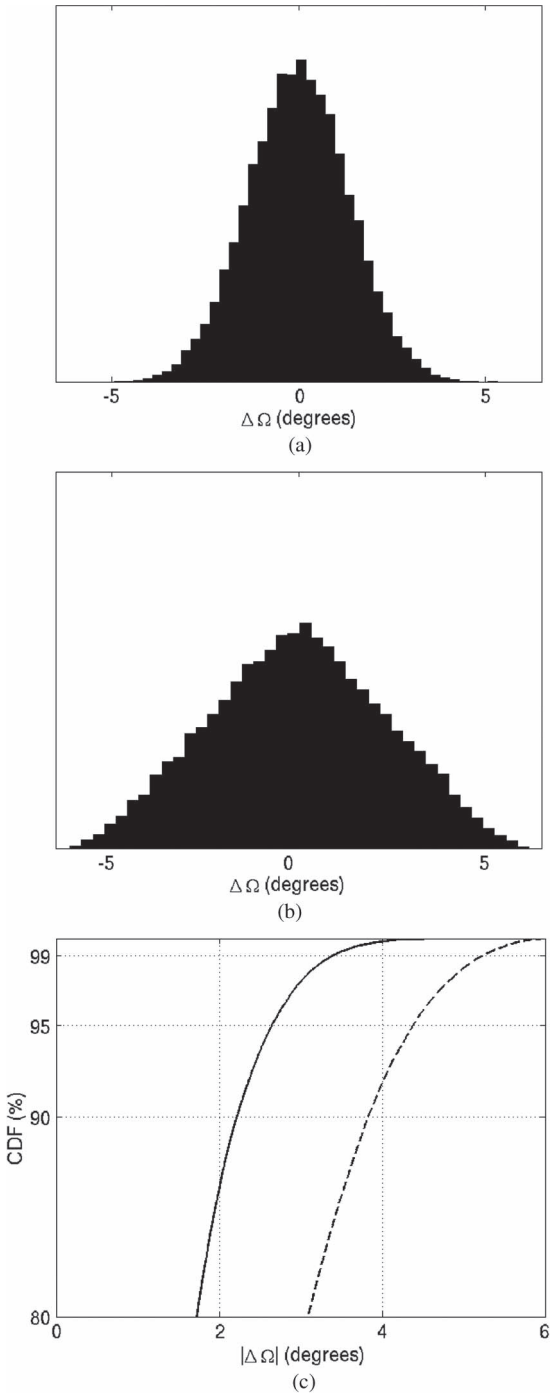

Fig. 3. (a) Histogram of the bias in Ω when $\Omega = 0$ for 50 000 random realizations of the system distortion with amplitudes < 0.1 and with no system noise. (b) Similar to (a) but with the system distortion amplitudes fixed at 0.1. (c) Cumulative distribution of the absolute bias corresponding to (a) (solid line) and (b) (dashed line). The calculations are for a biomass of 200 t $\cdot$ ha^{-1}.

that there is a 1% probability of the bias exceeding 3.4° when the amplitudes are treated as random, and exceeding 5.2° when the amplitudes are fixed at their largest permitted value of 0.1.

B. Maximum Bias in Faraday Rotation for Nonzero Values of Ω

In order to test whether the predictions are met for other values of Ω, the maximum biases derived from the numerical optimization for several values of Ω are given in Table III, along with the phases of the associated distortion terms; the amplitudes of the distortion terms are constrained not to exceed 0.1, and the noise is neglected. The channel imbalance is set to zero in the calculations in Table III(a) but is included in Table III(b). The optimization again confirms the first-order predictions that the distortion terms will all take their maximum permitted values and that $\arg(\delta_3) - \arg(\delta_1) = \arg(\delta_2) - \arg(\delta_4) \approx \pi$. In addition, $\arg(\varepsilon_1) \approx \arg(\varepsilon_2)$, although this relation is less accurately met for $\Omega = 0°$ and 90°. Note that, in Table III(a), the maximum biases occur when $\Omega = 0°$ or 90°, which reinforces the importance of the case where $\Omega = 0°$ considered in Section V-A.

TABLE III
MAXIMUM VALUES (IN DEGREES) OF THE FARADAY ROTATION BIAS DERIVED USING THE NUMERICAL OPTIMIZATION WHEN THE AMPLITUDES OF THE DISTORTION TERMS DO NOT EXCEED 0.1 AND WHEN THE NOISE IS NEGLECTED. (a) CHANNEL IMBALANCE ASSUMED NEGLIGIBLE. (b) ALL DISTORTION TERMS INCLUDED. THE AMPLITUDES OF THE DISTORTION TERMS ALL ASSUME THEIR MAXIMUM VALUE OF 0.1, WHEREAS THE PHASES ARE GIVEN IN THE TABLES. THE CALCULATIONS ARE FOR A BIOMASS OF 200 t $\cdot$ ha^{-1}

Ω	$\widehat{\Omega} - \Omega$	$\arg(\delta_1)$	$\arg(\delta_2)$	$\arg(\delta_3)$	$\arg(\delta_4)$
0	6.1	-166.5	-30.8	13.6	149.1
20	5.9	-168.9	-18.6	11.7	160.4
40	5.7	-179.1	-0.9	2.0	178.0
60	5.8	-10.2	-172.2	170.9	6.9
80	6.0	-27.5	-166.5	153.1	13.2
90	6.1	-30.9	-166.4	149.2	13.5

(a)

Ω	$\widehat{\Omega} - \Omega$	$\arg(\delta_1)$	$\arg(\delta_2)$	$\arg(\delta_3)$	$\arg(\delta_4)$	$\arg(\varepsilon_1)$	$\arg(\varepsilon_2)$
0	6.3	11.1	143.6	-168.6	-35.2	177.1	154.1
20	7.2	8.8	153.5	-170.8	-27.3	-158.5	-160.2
40	7.6	3.2	172.7	-175.9	-8.4	-153.4	-154.0
60	7.4	-12.9	-174.4	168.4	4.7	-146.2	-145.8
80	6.9	-26.6	-167.0	153.8	12.3	-151.1	-147.5
90	6.5	-25.8	-163.6	154.0	15.6	-178.0	-169.1

(b)

The behavior shown in Table III can be explained under the coarse assumption that all the distortion terms in the denominator of (17) are negligible compared with 1, which is equivalent to ignoring all second-order terms in the binomial expansion of (17). Then

$$E \approx u\cos\phi_3 + v\cos\phi_2 + pt\cos(\psi+\tau)\tilde{S} + t\tilde{C}\left(u\cos(\phi_3+\tau) - v\cos(\phi_2+\tau)\right) \quad (31)$$

where we have used the notation in (19). Using a similar approach to that in Section III-B, this can be written as

$$E = |1+\tilde{C}T|u\cos(\phi_3+\omega_3) + |1-\tilde{C}T|v\sin(\phi_2+\omega_2) + \tilde{S}tp\cos(\psi+\tau) \quad (32)$$

where

$$\omega_3 = \tan^{-1}\left(\frac{\tilde{C}t}{1+\tilde{C}t\cos\tau}\right) \quad \omega_2 = \tan^{-1}\left(\frac{1-t\tilde{C}\cos\tau}{t\tilde{C}}\right)$$

and T is defined in (18a). By choosing $\phi_2 = \pi/2 - \omega_2$, $\phi_3 = -\omega_3$, and $\psi = -\tau$ or $\pi - \tau$ (depending on the sign of $\tilde{S}$), E achieves its maximum positive value as follows:

$$E = 2\Delta\delta_M\left(|1+\tilde{C}T| + |1-\tilde{C}T|\right) + 2\Delta\varepsilon_M|\tilde{S}|t. \quad (33)$$

Before examining the behavior of E as a function of Ω, it helps to establish the range of values of its first term. Setting

$$R_1 = |1 + \tilde{C}T| = \sqrt{1 + \tilde{C}^2t^2 + 2\tilde{C}t\cos\tau}$$
$$R_2 = |1 - \tilde{C}T| = \sqrt{1 + \tilde{C}^2t^2 - 2\tilde{C}t\cos\tau}$$

then

$$\frac{d(R_1 + R_2)}{d\tau} = \tilde{C}t\sin\tau\left(-\frac{1}{R_1} + \frac{1}{R_2}\right). \quad (34)$$

If $\tilde{C} > 0$, then $R_1 \geq R_2$, whereas if $\tilde{C} < 0$, then $R_2 \geq R_1$. Hence, in either case, we have

$$\frac{d(R_1 + R_2)}{d\tau} \geq 0 \text{ for } 0 \leq \tau \leq \pi/2$$

and this derivative is 0 only when $\tau = 0$ or $\tau = \pi/2$. Since $R_1 + R_2$, as a function of τ, is symmetric about every multiple of $\pi/2$ and increases from a value of 2 when $\tau = 0$ to a value of $2\sqrt{1 + \tilde{C}^2t^2}$ at $\tau = \pi/2$, then $R_1 + R_2 \geq 2$ whatever the value of t, τ, and Ω.

Now, consider E in (33) as a function of Ω. Then

$$\frac{d(R_1 + R_2)}{d\Omega} = -2t\tilde{S}\left(\frac{\tilde{C}t + \cos\tau}{R_1} + \frac{\tilde{C}t - \cos\tau}{R_2}\right). \quad (35)$$

It is easy to show that, in the range $0 \leq \Omega \leq \pi/4$, $d(R_1 + R_2)/d\Omega = 0$ if and only if $\Omega = 0$ or $\pi/4$ (or if $\tau = k\pi$, in which case $R_1 + R_2 = 2$ whatever the value of Ω). Hence, $R_1 + R_2$ either continually increases or decreases over this range. However, when $\Omega = 0^\circ$, we have

$$R_1 + R_2 = \sqrt{1 + t^2 + 2t\cos\tau} + \sqrt{1 + t^2 - 2t\cos\tau} \geq 2$$

whatever the value of t and τ (with equality only if τ is a multiple of π or $t = 0$), whereas when $\Omega = \pi/4$, $R_1 + R_2 = 2$. Hence, $R_1 + R_2$ decreases as Ω increases from 0 to $\pi/4$. Furthermore, $R_1 + R_2$ is symmetric in Ω about every multiple of $\pi/4$; thus, it will increase from $\pi/4$ to $\pi/2$.

For the calculations in Table III, $t = 0.54$, and $\tau = -38.5^\circ$ [see Table I(b)]; thus, at $\Omega = 0^\circ$, $R_1 = 1.46$, $R_2 = 0.67$, and the range of $R_1 + R_2$ is only from 2 to 2.13. Substituting these values into (33) with $\Delta\delta_M = 0.1$ and $\Delta\varepsilon_M = 0$ yields Faraday rotation biases ranging between 5.45° and 5.76°. Hence, both the overall trend and the range of variation of the biases shown in Table III(a) are consistent with this analysis, although the absolute values of the bias are less than those found by the numerical optimization. These underestimates are unsurprising given the coarseness of approximation (31) and the fact that the errors in the amplitudes of the distortion terms are as large as 0.1.

For the full expression (33), E is symmetric about $\pi/4$ in the range $0 \leq \Omega \leq \pi/2$ and

$$\frac{dE}{d\Omega} = 2\Delta\delta_M\frac{d(R_1 + R_2)}{d\Omega} + 4\tilde{C}t\Delta\varepsilon_M. \quad (36)$$

When $\Omega = 0$, $dE/d\Omega = 4t\Delta\varepsilon_M > 0$, and when $\Omega = \pi/4$, $dE/d\Omega = 0$. However, whether the turning point at $\Omega = \pi/4$ is a maximum or a minimum depends on t and τ, as can be seen by examining the sign of the second derivative of E at this point. Writing

$$\frac{d(R_1 + R_2)}{d\Omega} = -2t\tilde{S}\left(\tilde{C}t\left\{\frac{1}{R_1} + \frac{1}{R_2}\right\} + \cos\tau\left\{\frac{1}{R_1} - \frac{1}{R_2}\right\}\right),$$

differentiating with respect to Ω, and using the facts that, when $\Omega = \pi/4$, $R_1 = R_2 = 1$, $dR_1/d\Omega = -2t\cos\tau$, and $dR_2/d\Omega = 2t\cos\tau$, then it is readily shown that, at this point

$$\frac{d^2(R_1 + R_2)}{d\Omega^2} = 4t^2(1 + \sin^2\tau).$$

From (36), we have

$$\frac{d^2E}{d\Omega^2} = 2\Delta\delta_M\frac{d^2(R_1 + R_2)}{d\Omega^2} - 8\tilde{S}t\Delta\varepsilon_M \quad (37)$$

which therefore takes the value $8t((1 + \sin^2\tau)t\Delta\delta_M - \Delta\varepsilon_M)$ at $\Omega = \pi/4$. For the calculations in Table III(b), $\Delta\delta_M = \Delta\varepsilon_M = 0.1$; thus, the second derivative (37) is negative, and the turning point is a maximum, i.e., the bias increases from its minimum at $\Omega = 0$ to its maximum value at $\Omega = \pi/4$, as shown in Table III(b). Since the range of the values of E is only from 0.426 to 0.508, we again only find a small range of variation in the bias, i.e., from 5.77° to 6.73°, and these approximate values are again underestimates of the values found by the numerical optimization.

The weak dependence of the maximum bias on Ω is a general property since the maximum value of $R_1 + R_2$ is $\sqrt{1 + t^2} + \sqrt{1 - t^2}$, which occurs when $\cos\tau = 0$. If the values of t in Table I(b) are typical, then $t < 1$, and $2 \leq R_1 + R_2 < 2\sqrt{2}$, which implies a variation of at most 20% in the Faraday rotation bias about its midvalue as Ω varies.

C. Constraining Maximum Faraday Rotation Bias

The aforementioned simulations all assume that the maximum amplitudes of the crosstalk and channel imbalance terms are the same and hence do not reveal the sensitivity of the maximum Faraday rotation bias to the individual types of distortions. To assess this, the combinations of the crosstalk and channel imbalance amplitudes giving rise to a defined maximum bias when $\Omega = 0$ were evaluated using simulation. These are displayed in the contour plot in Fig. 4, in which individual contours are labeled with the maximum bias in degrees; the calculations use covariance values appropriate to a biomass of 200 t · ha^{-1}.

Note that, except for the largest values of ε_M where the first-order approximation is no longer tenable, the behavior of this plot is very similar to that predicted by (30) when it is written in the following form:

$$(\Delta\delta_M)_{dB} = 20\log_{10} \times \left(\frac{\tan 4(\hat{\Omega} - \Omega)}{2}\frac{\left(1 - 2 \times 10^{(\Delta\delta_M)_{\mathrm{dB}}/20}|1 - T|\right)}{|1 + T| + |1 - T|}\right). \quad (38)$$

For example, when $\hat{\Omega} - \Omega = 1^\circ$, the value of $\Delta\delta_M$ predicted by (38) declines from -35.5 to -36.7 dB as $\Delta\varepsilon_M$ increases from -60 to -20 dB, whereas when $\hat{\Omega} - \Omega = 0.5^\circ$, the decline in $\Delta\delta_M$ over the same range of $\Delta\varepsilon_M$ is from -41.2 to -42.4 dB.

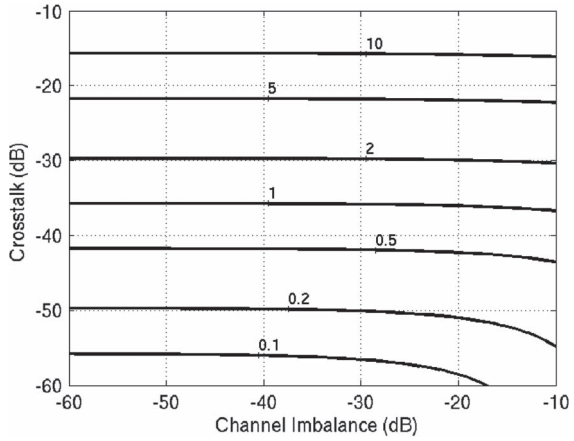

Fig. 4. Contour plot derived from the simulation showing the combinations of the crosstalk and the channel imbalance that give rise to the given maximum Faraday rotation bias when $\Omega = 0$; the bias in degrees is marked on the contours. The calculations are for a biomass of 200 t $\cdot$ ha^{-1}.

It is apparent that, while the bias in Ω depends on the channel imbalance, as shown by (17), the key control on its *maximum possible value* is the crosstalk amplitude. Unless the crosstalk is less than -35 dB, the maximum bias is nearly independent of the amplitude of the channel imbalance term. This plot also makes clear that keeping the maximum bias as low as 1.2°, as recommended in [12], requires the crosstalk terms to have an amplitude less than around -35 dB. However, as Fig. 3(c) indicates, this requirement will be less demanding if we accept a 99% probability of the maximum bias being less than 1.2°. The requirement that the Faraday rotation bias be less than 5°, as suggested in [2] and [3], will *always* be met if the crosstalk amplitude does not exceed -21.4 dB. This condition will depend on the covariance matrix, as shown by (38), but for the three covariance matrices considered, the variation is slight, i.e., the corresponding values for 50 and 350 t $\cdot$ ha^{-1} are -21.1 and -21.2 dB, respectively.

VI. Conclusion

This paper has provided a first-order differentiable approximation to the bias in Faraday rotation estimates caused by system distortions and noise, from which the conditions on the amplitudes and phases of the crosstalk and channel imbalance terms that give rise to the largest possible bias in Ω are derived, given the constraints on the amplitude of the distortion terms. In addition to confirming the predictions from the analysis, simulation allows the statistical properties of the estimate to be investigated when the amplitudes and phases of the distortion terms are treated as random variables. In particular, the cumulative density function of the Faraday rotation bias can be empirically derived so that the likelihood of the bias exceeding a given threshold can be quantified.

The following are demonstrated.

1) The phases of the distortion terms have significant effects on the size of the Faraday rotation bias, and the largest bias occurs for particular phase relationships between the distortion terms. These worst case phases depend on the target covariance, thus varying across a scene, as does the size of the maximum possible bias. However, the maximum bias only exhibits a weak variation over the range of covariance matrices considered in this paper.
2) When $\Omega = 0$, a bias exceeding 1.9° can occur even when the distortion amplitudes are as small as 0.0316 (-30 dB). This makes it hard to guarantee that the bias should not exceed 1.2°, as proposed in [12]. The condition on the crosstalk amplitude would be less stringent, however, if we only require, e.g., a 99% probability that the bias should not exceed 1.2°.
3) The maximum Faraday rotation bias can be constrained by assigning a maximum amplitude just to the crosstalk since the maximum bias is very insensitive to the amplitude of the channel imbalance terms.

This paper has focused on the bias in the Faraday rotation estimate and hence has not considered the uncertainty arising from the window size used in the estimate, i.e., the number of looks. This uncertainty is effectively absent from the simulations since they use 10 000 looks to represent the scene, but it can be readily investigated, at the cost of computer time, using simulation.

The presence of bias in the Faraday rotation estimates can be most easily investigated near the magnetic equator. This is because, from (1), the Faraday rotation is zero if the angle between the radar beam and the geomagnetic field is 90°. This condition will be met in some equatorial locations for a polar-orbiting satellite orbit. The nonzero estimates of the Faraday rotation at these locations indicate the presence of bias, which will affect all measurements along the orbit.

Finally, the simulations in this paper have not made any assumptions about how accurately calibration procedures can estimate the system distortion terms and, hence, what the realistic constraints on their amplitudes are. For the Phased Array type L-band SAR (PALSAR), this has been addressed in [21] and [23], where values of the crosstalk less than -35 dB were found; from (38), this corresponds to a maximum Faraday rotation bias of 1.08°. Significant channel imbalance was found, but this was largely removed by calibration and is not of major importance as regards the maximum bias (see Section V). Further opportunities to assess the L-band system distortion both before and after calibration and its effects on the estimation of the Faraday rotation will be provided by the Advanced Land Observing Satellite-2 (ALOS-2) and the Argentine Microwaves Observation Satellite (SAOCOM) radars, but our first chance to carry out similar studies at P-band awaits the launch of BIOMASS.

Appendix
First-Order Estimate of Faraday Rotation Bias

$$A_1 = S_{\mathrm{hv}}\Sigma_\delta - cs\,(S_{\mathrm{hh}} + S_{\mathrm{vv}})\,(X_{31} + X_{24}) \tag{A1a}$$

$$\begin{aligned} B_1 &= S_{\mathrm{hh}}(c^2 X_{31} - s^2 X_{24}) + S_{\mathrm{vv}}(c^2 X_{24} - s^2 X_{31}) \\ &= X_{31}(c^2 S_{\mathrm{hh}} - s^2 S_{\mathrm{vv}}) + X_{24}(c^2 S_{\mathrm{vv}} - s^2 S_{\mathrm{hh}}) \end{aligned} \tag{A1b}$$

$$A_2 = (-s^2 S_{\mathrm{hh}} + c^2 S_{\mathrm{vv}})\Sigma_\varepsilon \tag{A2a}$$

$$B_2 = S_{\mathrm{hv}} Y_{21} + cs(S_{\mathrm{hh}} + S_{\mathrm{vv}})\Sigma_\varepsilon \tag{A2b}$$

$$
\begin{aligned}
&(A+jB)(A_1-jB_1)^*+(A-jB)^*(A_1+jB_1)\\
&=e^{2j\Omega}\left(S_{\rm hh}+S_{\rm vv}\right)\left(S_{\rm hv}\Sigma_\delta-e^{-j\Omega}\left\{X_{31}(jcS_{\rm hh}+sS_{\rm vv})+X_{24}(sS_{\rm hh}+jcS_{\rm vv})\right\}\right)^*\\
&\quad+e^{2j\Omega}\left(S_{\rm hh}+S_{\rm vv}\right)^*\left(S_{\rm hv}\Sigma_\delta+e^{j\Omega}\left\{X_{31}(jcS_{\rm hh}-sS_{\rm vv})+X_{24}(-sS_{\rm hh}+jcS_{\rm vv})\right\}\right)\\
&=2e^{2j\Omega}{\rm Re}\left\{\left(S_{\rm hh}+S_{\rm vv}\right)S_{\rm hv}^*\Sigma_\delta^*\right\}\\
&\quad+e^{3j\Omega}\left\{X_{31}(S_{\rm hh}+S_{\rm vv})^*(jcS_{\rm hh}-sS_{\rm vv})-X_{31}^*(S_{\rm hh}+S_{\rm vv})(-jcS_{\rm hh}^*+sS_{\rm vv}^*)\right\}\\
&\quad+e^{3j\Omega}\left\{X_{24}(S_{\rm hh}+S_{\rm vv})^*(-sS_{\rm hh}+jcS_{\rm vv})-X_{24}^*(S_{\rm hh}+S_{\rm vv})(sS_{\rm hh}^*-jcS_{\rm vv}^*)\right\}
\end{aligned}
\tag{A9}
$$

where

$$
\begin{aligned}
X_{31}&=\Delta\delta_3-\Delta\delta_1\equiv P+jQ\\
X_{24}&=\Delta\delta_2-\Delta\delta_4\equiv U+jV\\
\Sigma_\delta&=\Delta\delta_1+\Delta\delta_2+\Delta\delta_3+\Delta\delta_4\\
Y_{21}&=\Delta\varepsilon_2-\Delta\varepsilon_1\\
\Sigma_\varepsilon&=\Delta\varepsilon_2+\Delta\varepsilon_1\equiv C+jD.
\end{aligned}
\tag{A3}
$$

Hence

$$
\begin{aligned}
A_1+jB_1=&S_{\rm hv}\Sigma_\delta\\
&+X_{31}\left\{-cs\left(S_{\rm hh}+S_{\rm vv}\right)+j(c^2S_{\rm hh}-s^2S_{\rm vv})\right\}\\
&+X_{24}\left\{-cs\left(S_{\rm hh}+S_{\rm vv}\right)+j(c^2S_{\rm vv}-s^2S_{\rm hh})\right\}\\
=&S_{\rm hv}\Sigma_\delta\\
&+e^{j\Omega}\left\{X_{31}(jcS_{\rm hh}-sS_{\rm vv})+X_{24}(-sS_{\rm hh}+jcS_{\rm vv})\right\}.
\end{aligned}
\tag{A4a}
$$

Similarly

$$
\begin{aligned}
A_1-jB_1=&S_{\rm hv}\Sigma_\delta\\
&-e^{-j\Omega}\{X_{31}(jcS_{\rm hh}+sS_{\rm vv})+X_{24}(sS_{\rm hh}+jcS_{\rm vv})\}.
\end{aligned}
\tag{A4b}
$$

In addition

$$
A_2+jB_2=jS_{\rm hv}Y_{21}+e^{j\Omega}(jsS_{\rm hh}+cS_{\rm vv})\Sigma_\varepsilon \tag{A5a}
$$

$$
A_2-jB_2=-jS_{\rm hv}Y_{21}+e^{-j\Omega}\left(-jsS_{\rm hh}+cS_{\rm vv}\right)\Sigma_\varepsilon. \tag{A5b}
$$

Expanding $(\hat{A}+j\hat{B})^*(\hat{A}-j\hat{B})$ and discarding the quadratic terms leads to the following expression:

$$
\begin{aligned}
Z_1Z_2^*=&(\hat{A}+j\hat{B})(\hat{A}-j\hat{B})^*\\
\approx&(A+jB)(A-jB)^*+(A+jB)(A_1-jB_1)^*\\
&+(A+jB)(A_2-jB_2)^*+(A-jB)^*(A_1+jB_1)\\
&+(A-jB)^*(A_2+jB_2).
\end{aligned}
\tag{A6}
$$

The noise terms are omitted since they occur in products with the signal and in the following product:

$$
\begin{aligned}
&(\mathbf{N'}_{\rm hh}+\mathbf{N'}_{\rm vv}+j(\mathbf{N'}_{\rm vh}-\mathbf{N'}_{\rm hv}))\\
&\qquad\times(\mathbf{N'}_{\rm hh}+\mathbf{N'}_{\rm vv}+j\left(\mathbf{N'}_{\rm vh}-\mathbf{N'}_{\rm hv}\right))^*.
\end{aligned}
$$

Hence, if the noise terms are uncorrelated with the signal and with each other, and are of equal power, the expected value of all terms containing noise is 0.

Since

$$
\begin{aligned}
A+jB=&e^{2j\Omega}\left(S_{\rm hh}+S_{\rm vv}\right)\\
A-jB=&e^{-2j\Omega}\left(S_{\rm hh}+S_{\rm vv}\right)
\end{aligned}
\tag{A7}
$$

the first term in (A6) can be written as

$$
(A+jB)(A-jB)^*=e^{4j\Omega}\left|S_{\rm hh}+S_{\rm vv}\right|^2. \tag{A8}
$$

The terms involving δ are given in (A9), shown at the top of the page.

Averaging over looks and using the notation in (A3), the terms involving X_{31} can be written as

$$
\begin{aligned}
&X_{31}\left\langle(S_{\rm hh}+S_{\rm vv})^*(jcS_{\rm hh}-sS_{\rm vv})\right\rangle\\
&\quad-X_{31}^*\left\langle(S_{\rm hh}+S_{\rm vv})(-jcS_{\rm hh}^*+sS_{\rm vv}^*)\right\rangle\left(S_{\rm hh}+S_{\rm vv}\right)\\
&=(P+jQ)(jc\sigma_{\rm hh}-s\sigma_{\rm vv}+R[jce^{j\theta}-se^{-j\theta}])\\
&\quad+(P-jQ)(jc\sigma_{\rm hh}-s\sigma_{\rm vv}+R[-se^{j\theta}+jce^{-j\theta}])\\
&=2P(jc\sigma_{\rm hh}-s\sigma_{\rm vv}+jR{\rm e}^{j\Omega}\cos\theta)-2jQR{\rm e}^{-j\Omega}\sin\theta
\end{aligned}
\tag{A10}
$$

where $\sigma_{\rm pp}=\langle|S_{\rm pp}|^2\rangle$, and $\langle S_{\rm hh}S_{\rm vv}^*\rangle=R{\rm e}^{j\theta}$.

The corresponding expression for X_{24} is

$$
\begin{aligned}
&X_{24}\left\langle(S_{\rm hh}+S_{\rm vv})^*(-sS_{\rm hh}+jcS_{\rm vv})\right\rangle\\
&\quad-X_{24}^*\left\langle(S_{\rm hh}+S_{\rm vv})(sS_{\rm hh}^*-jcS_{\rm vv}^*)\right\rangle\\
&=2U(-s\sigma_{\rm hh}+jc\sigma_{\rm vv}+Rje^{j\Omega}\cos\theta)+2jVR{\rm e}^{-j\Omega}\sin\theta.
\end{aligned}
\tag{A11}
$$

Similarly, for the channel imbalance terms, we have

$$
\begin{aligned}
&(A+jB)(A_2-jB_2)^*+(A-jB)^*(A_2+jB_2)\\
&=e^{2j\Omega}\left(S_{\rm hh}+S_{\rm vv}\right)\left(-jS_{\rm hv}Y_{21}+e^{-j\Omega}\left(-jsS_{\rm hh}+cS_{\rm vv}\right)\Sigma_\varepsilon\right)^*\\
&\quad+e^{2j\Omega}\left(S_{\rm hh}+S_{\rm vv}\right)^*\left(jS_{\rm hv}Y_{21}+e^{j\Omega}(jsS_{\rm hh}+cS_{\rm vv})\Sigma_\varepsilon\right)\\
&=je^{2j\Omega}2{\rm Re}\left(\left(S_{\rm hh}+S_{\rm vv}\right)S_{\rm hv}^*Y_{21}^*\right)\\
&\quad+e^{3j\Omega}\left((C-jD)(S_{\rm hh}+S_{\rm vv})(jsS_{\rm hh}^*+cS_{\rm vv}^*)\right.\\
&\qquad\left.+(C+jD)(S_{\rm hh}+S_{\rm vv})^*(jsS_{\rm hh}+cS_{\rm vv})\right).
\end{aligned}
\tag{A12}
$$

After averaging, the coefficient of $e^{3j\Omega}$ can be more simply written as

$$\begin{aligned}
&\langle (C-jD)(S_{\rm hh}+S_{\rm vv})\,(jsS_{\rm hh}^*+cS_{\rm vv}^*)\\
&\quad +(C+jD)(S_{\rm hh}+S_{\rm vv})^*(jsS_{\rm hh}+cS_{\rm vv})\rangle\\
&=(C+jD)\left(js\sigma_{\rm hh}+c\sigma_{\rm vv}+R[jse^{j\theta}+ce^{-j\theta}]\right)\\
&\quad +(C-jD)\left(js\sigma_{\rm hh}+c\sigma_{\rm vv}+R[ce^{j\theta}+jse^{-j\theta}]\right)\\
&=C(2js\sigma_{\rm hh}+2c\sigma_{\rm vv}+2R{\rm e}^{j\Omega}\cos\theta)+2DR{\rm e}^{-j\Omega}\sin\theta
\end{aligned} \tag{A13}$$

Gathering the terms, we find

$$\begin{aligned}
&\left\langle (\hat{A}+j\hat{B})(\hat{A}-j\hat{B})^*\right\rangle\\
&\approx e^{4j\Omega}\left(\left\langle |S_{hh}+S_{vv}|^2\right\rangle+2R\cos\theta(jP+jU+C)\right)+2e^{3j\Omega}\\
&\quad\times(P(jc\sigma_{hh}-s\sigma_{vv})+U(-s\sigma_{hh}+jc\sigma_{vv})\\
&\qquad +C(js\sigma_{hh}+c\sigma_{vv}))\\
&\quad +2e^{2j\Omega}R\sin\theta(-jQ+jV+D)+2e^{2j\Omega}\\
&\quad\times\langle{\rm Re}\left((S_{hh}+S_{vv})S_{hv}^*\Sigma_\delta^*\right)+j{\rm Re}\left((S_{hh}+S_{vv})S_{hv}^*Y_{21}^*\right)\rangle
\end{aligned} \tag{A14}$$

Hence

$$\begin{aligned}
&\left\langle\left|\hat{Z}_1\hat{Z}_2^*\right|\cos 4\hat{\Omega}\right\rangle=\cos 4\Omega\left(\left\langle|S_{\rm hh}+S_{\rm vv}|^2\right\rangle+2RC\cos\theta\right)\\
&\quad -\sin 4\Omega\,(2(P+U)R\cos\theta)\\
&\quad +2\cos 3\Omega(-sP\sigma_{\rm vv}-sU\sigma_{\rm hh}+cC\sigma_{\rm vv})\\
&\quad -2\sin 3\Omega(cP\sigma_{\rm hh}+cU\sigma_{\rm vv}+sC\sigma_{\rm hh})\\
&\quad +2R\sin\theta\,(D\cos 2\Omega+(Q-V)\sin 2\Omega)\\
&\quad +2\cos 2\Omega{\rm Re}\left\langle(S_{\rm hh}+S_{\rm vv})\,S_{\rm hv}^*\Sigma_\delta^*\right\rangle\\
&\quad -2\sin 2\Omega{\rm Re}\left\langle(S_{\rm hh}+S_{\rm vv})\,S_{\rm hv}^*Y_{21}^*\right\rangle
\end{aligned} \tag{A15}$$

$$\begin{aligned}
&\left\langle\left|\hat{Z}_1\hat{Z}_2^*\right|\sin 4\hat{\Omega}\right\rangle=\sin 4\Omega\left(\left\langle|S_{\rm hh}+S_{\rm vv}|^2\right\rangle+2RC\cos\theta\right)\\
&\quad +\cos 4\Omega\,(2(P+U)R\cos\theta)\\
&\quad +2\sin 3\Omega(-sP\sigma_{\rm vv}-sU\sigma_{\rm hh}+cC\sigma_{\rm vv})\\
&\quad +2\cos 3\Omega(cP\sigma_{\rm hh}+cU\sigma_{\rm vv}+sC\sigma_{\rm hh})\\
&\quad +2R\sin\theta\,\{D\sin 2\Omega-(Q-V)\cos 2\Omega\}\\
&\quad +2\sin 2\Omega{\rm Re}\left\langle(S_{\rm hh}+S_{\rm vv})\,S_{\rm hv}^*\Sigma_\delta^*\right\rangle\\
&\quad +2\cos 2\Omega{\rm Re}\left\langle(S_{\rm hh}+S_{\rm vv})\,S_{\rm hv}^*Y_{21}^*\right\rangle.
\end{aligned} \tag{A16}$$

Now, using

$$\begin{aligned}
2\sin 3\Omega\cos\Omega&=\sin 4\Omega+\sin 2\Omega\\
2\cos 3\Omega\sin\Omega&=\sin 4\Omega-\sin 2\Omega\\
2\cos 3\Omega\cos\Omega&=\cos 4\Omega+\cos 2\Omega\\
2\sin 3\Omega\sin\Omega&=-\cos 4\Omega+\cos 2\Omega
\end{aligned}$$

the middle lines of (A15) become

$$\begin{aligned}
&-(\sin 4\Omega-\sin 2\Omega)(P\sigma_{\rm vv}+U\sigma_{\rm hh})+(\cos 4\Omega+\cos 2\Omega)C\sigma_{\rm vv}\\
&-(\sin 4\Omega+\sin 2\Omega)(P\sigma_{\rm hh}+U\sigma_{\rm vv})-(-\cos 4\Omega+\cos 2\Omega)C\sigma_{\rm hh}.
\end{aligned}$$

Hence

$$\begin{aligned}
&\left\langle\left|\hat{Z}_1\hat{Z}_2^*\right|\cos 4\hat{\Omega}\right\rangle\\
&=\cos 4\Omega\left(\left\langle|S_{\rm hh}+S_{\rm vv}|^2\right\rangle+C\sigma_{\rm vv}+C\sigma_{\rm hh}+2RC\cos\theta\right)\\
&\quad -\sin 4\Omega\,(2(P+U)R\cos\theta+P\sigma_{\rm vv}+U\sigma_{\rm hh}+P\sigma_{\rm hh}+U\sigma_{\rm vv})\\
&\quad +\cos 2\Omega\,(2DR\sin\theta+C\sigma_{\rm vv}-C\sigma_{\rm hh})\\
&\quad +\sin 2\Omega\,(2(Q-V)R\sin\theta+P\sigma_{\rm vv}+U\sigma_{\rm hh}-(P\sigma_{\rm hh}+U\sigma_{\rm vv}))\\
&\quad +2\cos 2\Omega{\rm Re}\left\langle(S_{\rm hh}+S_{\rm vv})\,S_{\rm hv}^*\Sigma_\delta^*\right\rangle\\
&\quad -2\sin 2\Omega{\rm Re}\left\langle(S_{\rm hh}+S_{\rm vv})\,S_{\rm hv}^*Y_{21}^*\right\rangle
\end{aligned}$$

which can be written as

$$\begin{aligned}
&\left\langle\left|\hat{Z}_1\hat{Z}_2^*\right|\cos 4\hat{\Omega}\right\rangle\\
&=\left\langle|S_{\rm hh}+S_{\rm vv}|^2\right\rangle((1+C)\cos 4\Omega-(P+U)\sin 4\Omega)\\
&\quad +\cos 2\Omega\,(2DR\sin\theta+C(\sigma_{\rm vv}-\sigma_{\rm hh}))\\
&\quad +\sin 2\Omega\,(2(Q-V)R\sin\theta+(P-U)(\sigma_{\rm vv}-\sigma_{\rm hh}))\\
&\quad +2\cos 2\Omega{\rm Re}\left\langle(S_{\rm hh}+S_{\rm vv})\,S_{\rm hv}^*\Sigma_\delta^*\right\rangle\\
&\quad -2\sin 2\Omega{\rm Re}\left\langle(S_{\rm hh}+S_{\rm vv})\,S_{\rm hv}^*Y_{21}^*\right\rangle.
\end{aligned} \tag{A17}$$

Similarly

$$\begin{aligned}
&\left\langle\left|\hat{Z}_1\hat{Z}_2^*\right|\sin 4\hat{\Omega}\right\rangle\\
&=\left\langle|S_{\rm hh}+S_{\rm vv}|^2\right\rangle((1+C)\sin 4\Omega+(P+U)\cos 4\Omega)\\
&\quad +\sin 2\Omega\,(2DR\sin\theta+C(\sigma_{\rm vv}-\sigma_{\rm hh}))\\
&\quad -\cos 2\Omega\,(2(Q-V)R\sin\theta+(P-U)(\sigma_{\rm vv}-\sigma_{\rm hh}))\\
&\quad +2\sin 2\Omega{\rm Re}\left\langle(S_{\rm hh}+S_{\rm vv})\,S_{\rm hv}^*\Sigma_\delta^*\right\rangle\\
&\quad +2\cos 2\Omega\left\langle(S_{\rm hh}+S_{\rm vv})\,S_{\rm hv}^*Y_{21}^*\right\rangle.
\end{aligned} \tag{A18}$$

Equations (A17) and (A18) can be combined to give $\langle|\hat{Z}_1\hat{Z}_2^*|\exp(4j\hat{\Omega})\rangle$.

Setting

$$\begin{aligned}
L&=\left\langle|S_{\rm hh}+S_{\rm vv}|^2\right\rangle\\
J&=\cos 2\Omega\,(2DR\sin\theta+C(\sigma_{\rm vv}-\sigma_{\rm hh}))\\
&\quad +\sin 2\Omega\,(2(Q-V)R\sin\theta+(P-U)(\sigma_{\rm vv}-\sigma_{\rm hh}))\\
K&=\sin 2\Omega\,(2DR\sin\theta+C(\sigma_{\rm vv}-\sigma_{\rm hh}))\\
&\quad -\cos 2\Omega\,(2(Q-V)R\sin\theta+(P-U)(\sigma_{\rm vv}-\sigma_{\rm hh}))\\
M&=2{\rm Re}\left\langle(S_{\rm hh}+S_{\rm vv})\,S_{\rm hv}^*\Sigma_\delta^*\right\rangle\\
N&=2{\rm Re}\left\langle(S_{\rm hh}+S_{\rm vv})\,S_{\rm hv}^*Y_{21}^*\right\rangle
\end{aligned}$$

$$\begin{aligned}
&\tan(4\hat{\Omega}-4\Omega)\\
&=\frac{P+U+\frac{1}{L}\mathrm{Re}\left\{\langle(S_{\mathrm{vv}}+S_{\mathrm{hh}})^*(S_{\mathrm{vv}}-S_{\mathrm{hh}})\rangle\,(-\Sigma_\varepsilon\sin 2\Omega+(X_{24}-X_{31})\cos 2\Omega)+2\,\langle(S_{\mathrm{hh}}+S_{\mathrm{vv}})\,S_{\mathrm{hv}}^*\rangle\,(-\Sigma_\delta^*\sin 2\Omega+Y_{21}^*\cos 2\Omega)\right\}}{1+C+\frac{1}{L}\mathrm{Re}\left\{\langle(S_{\mathrm{vv}}+S_{\mathrm{hh}})^*(S_{\mathrm{vv}}-S_{\mathrm{hh}})\rangle\,(\Sigma_\varepsilon\cos 2\Omega+(X_{24}-X_{31})\sin 2\Omega)+2\langle(S_{\mathrm{hh}}+S_{\mathrm{vv}})\,S_{\mathrm{hv}}^*\rangle\,(\Sigma_\delta^*\cos 2\Omega+Y_{21}^*\sin 2\Omega)\right\}}\\
&=\frac{\mathrm{Re}\left\{X_{31}+X_{24}+T\,(\Sigma_\varepsilon\sin 2\Omega+(X_{31}-X_{24})\cos 2\Omega)+2W(-\Sigma_\delta^*\sin 2\Omega+Y_{21}^*\cos 2\Omega)\right\}}{1+\mathrm{Re}\left\{\Sigma_\varepsilon+T\,(-\Sigma_\varepsilon\cos 2\Omega+(X_{31}-X_{24})\sin 2\Omega)+2W(\Sigma_\delta^*\cos 2\Omega+Y_{21}^*\sin 2\Omega)\right\}}
\end{aligned}\tag{A21}$$

and using $\tan(A-B)=(\tan A-\tan B)/(1+\tan A\tan B)$, then

$$\begin{aligned}
&\tan(4\hat{\Omega}-4\Omega)\\
&=\frac{\frac{(1+C)\sin 4\Omega+(P+U)\cos 4\Omega+(K+M\sin 2\Omega+N\cos 2\Omega)/L}{(1+C)\cos 4\Omega-(P+U)\sin 4\Omega+(J+M\cos 2\Omega-N\sin 2\Omega)/L}-\frac{\sin 4\Omega}{\cos 4\Omega}}{1+\frac{(1+C)\sin 4\Omega+(P+U)\cos 4\Omega+(K+M\sin 2\Omega+N\cos 2\Omega)/L}{(1+C)\cos 4\Omega-(P+U)\sin 4\Omega+(J+M\cos 2\Omega-N\sin 2\Omega)/L}\frac{\sin 4\Omega}{\cos 4\Omega}}.
\end{aligned}\tag{A19}$$

Since

$$\begin{aligned}
&K\cos 4\Omega-J\sin 4\Omega\\
&=\cos 4\Omega\,(\sin 2\Omega\,\{2DR\sin\theta+C(\sigma_{\mathrm{vv}}-\sigma_{\mathrm{hh}})\}\\
&\quad-\cos 2\Omega\,\{2(Q-V)R\sin\theta+(P-U)(\sigma_{\mathrm{vv}}-\sigma_{\mathrm{hh}})\})\\
&\quad-\sin 4\Omega\,(\cos 2\Omega\,\{2DR\sin\theta+C(\sigma_{\mathrm{vv}}-\sigma_{\mathrm{hh}})\}\\
&\quad+\sin 2\Omega\,\{2(Q-V)R\sin\theta+(P-U)(\sigma_{\mathrm{vv}}-\sigma_{\mathrm{hh}})\})\\
&=-\{2DR\sin\theta+C(\sigma_{\mathrm{vv}}-\sigma_{\mathrm{hh}})\}\sin 2\Omega\\
&\quad-\{2(Q-V)R\sin\theta+(P-U)(\sigma_{\mathrm{vv}}-\sigma_{\mathrm{hh}})\}\cos 2\Omega\\
&=-\mathrm{Re}\,\{\langle(S_{\mathrm{vv}}+S_{\mathrm{hh}})^*(S_{\mathrm{vv}}-S_{\mathrm{hh}})\rangle\\
&\qquad\times\,(\Sigma_\varepsilon\sin 2\Omega+(X_{31}-X_{24})\cos 2\Omega)\}
\end{aligned}\tag{A20a}$$

and similarly

$$\begin{aligned}
&K\sin 4\Omega+J\cos 4\Omega\\
&\quad=\mathrm{Re}\,(\langle(S_{\mathrm{vv}}+S_{\mathrm{hh}})^*(S_{\mathrm{vv}}-S_{\mathrm{hh}})\rangle\\
&\qquad\times\,(\Sigma_\varepsilon\cos 2\Omega-(X_{31}-X_{24})\sin 2\Omega))
\end{aligned}\tag{A20b}$$

(A19) simplifies to (A21), shown at the top of the page, where

$$T=-\frac{\langle(S_{\mathrm{vv}}+S_{\mathrm{hh}})^*(S_{\mathrm{vv}}-S_{\mathrm{hh}})\rangle}{\left\langle|S_{\mathrm{hh}}+S_{\mathrm{vv}}|^2\right\rangle}$$

$$=\frac{\sigma_{\mathrm{hh}}-\sigma_{\mathrm{vv}}+2jR\sin\theta}{\sigma_{\mathrm{hh}}+\sigma_{\mathrm{vv}}+2R\cos\theta}\tag{A22a}$$

$$W=\frac{\langle(S_{\mathrm{hh}}+S_{\mathrm{vv}})\,S_{\mathrm{hv}}^*\rangle}{\left\langle|S_{\mathrm{hh}}+S_{\mathrm{vv}}|^2\right\rangle}.\tag{A22b}$$

ACKNOWLEDGMENT

The authors would like to thank the reviewers for their helpful questions and comments that led to a much improved paper.

REFERENCES

[1] M. P. M. Hall, L. W. Barclay, and M. T. Hewitt, Eds. *Propagation of Radiowaves*. London, U.K.: The Institution of Electrical Engineers, 1996.

[2] P. A. Wright, S. Quegan, N. S. Wheadon, and C. D. Hall, "Faraday rotation effects on L-band spaceborne SAR data," *IEEE Trans. Geosci. Remote Sens.*, vol. 41, no. 12, pp. 2735–2744, Dec. 2003.

[3] A. Freeman and S. S. Saatchi, "On the detection of Faraday rotation in linearly polarized L-band SAR backscatter signatures," *IEEE Trans. Geosci. Remote Sens.*, vol. 42, no. 8, pp. 1607–1616, Aug. 2004.

[4] S. Quegan *et al.*, Report for Mission Selection: Biomass, Eur. Space Agency, Noordwijk, The Netherlands, ESA SP 1324/1 (vol. 3), 2012.

[5] S. H. Bickel and R. H. T. Bates, "Effects of magneto-ionic propagation on the polarization scattering matrix," *Proc. IRE*, vol. 53, no. 8, pp. 1089–1091, Aug. 1965.

[6] A. Freeman, "Calibration of linearly polarized polarimetric SAR data subject to Faraday rotation," *IEEE Trans. Geosci. Remote Sens.*, vol. 42, no. 8, pp. 1617–1624, Aug. 2004.

[7] R.-Y. Qi and Y.-Q. Jin, "Analysis of the effects of Faraday rotation on spaceborne polarimetric SAR observations at P-Band," *IEEE Trans. Geosci. Remote Sens.*, vol. 45, no. 5, pp. 1115–1122, May 2007.

[8] J. Chen and S. Quegan, "Improved estimators of Faraday rotation in spaceborne polarimetric SAR data," *IEEE Geosci. Remote Sens. Lett.*, vol. 7, no. 4, pp. 846–850, Oct. 2010.

[9] C. Senior *et al.*, "*E* and *F* region study of the evening sector auroral oval: A Chatanika/Dynamics Explorer 2/NOAA 6 comparison," *J. Geophys. Res."Space Phys.*, vol. 92, no. A3, pp. 2477–2494, Mar. 1987.

[10] J. S. Kim, K. P. Papathanassiou, S. Quegan, and N. Rogers, "Estimation and correction of scintillation effects on spaceborne P-band SAR images," in *Proc. IEEE Int. Geosci. Remote Sens. Symp.*, Munich, Germany, pp. 5101–5104, Jul. 22–27, 2012.

[11] J. S. Kim, K. P. Papathanassiou, R. Scheiber, and S. Quegan, "Correction of ionospheric scintillation induced distortions on polarimetric SAR data," *IEEE Trans. Geosci. Remote Sens.*, to be published.

[12] F. J. Meyer and J. B. Nicoll, "Prediction, detection, and correction of Faraday rotation in full-polarimetric L-band SAR data," *IEEE Trans. Geosci. Remote Sens.*, vol. 46, no. 10, pp. 3076–3086, Oct. 2008.

[13] N. C. Rogers and S. Quegan, "The accuracy of Faraday rotation estimation in satellite synthetic aperture radar images," *IEEE Trans. Geosci. Remote Sens.*, vol. 52, no. 8, pp. 4799–4807, Aug. 2014.

[14] J. S. Kim and K. P. Papathanassiou, "Faraday rotation estimation performance analysis," in *Proc. 8th EUSAR Conf.*, Aachen, Germany, Jun. 7–10, 2010, pp. 182–185.

[15] N. R. Goodman, "Statistical analysis based on a certain multivariate Gaussian distribution (An introduction)," *Ann. Math. Stat.*, vol. 34, no. 1, pp. 152–177, Mar. 1963.

[16] J. Chen, S. Quegan, and X. J. Yin, "Calibration of spaceborne linearly polarized low frequency SAR using polarimetric selective radar calibrators," *Progr. Electromagn. Res.*, vol. 114, pp. 89–111, 2011.

[17] A. Freeman, X. Pi, and B. Chapman, "Calibration of PALSAR polarimetric data," presented at the 4th Int. Workshop Science Applications SAR Polarimetric Interferometry—PolInSAR, Frascati, Italy, Jan. 26–30, 2009, Paper ESA SP-668.

[18] S. Quegan and M. R. Lomas, "The interaction between Faraday rotation and system effects in synthetic aperture radar measurements of backscatter and biomass," *IEEE Trans. Geosci. Remote Sens.*, vol. 53, no. 8, pp. 4299–4312, Aug. 2015.
[19] M. Fujita, "Polarimetric calibration of space SAR data subject to Faraday rotation—A three target approach," in *Proc. IEEE IGARSS*, Seoul, Korea, 2005, pp. 5497–5500.
[20] H. Kimura, "Calibration of polarimetric PALSAR imagery affected by Faraday rotation using polarization orientation," *IEEE Trans. Geosci. Remote Sens.*, vol. 47, no. 12, pp. 3943–3950, Dec. 2009.
[21] M. Shimada, O. Isoguchi, T. Tadono, and K. Isono, "PALSAR radiometric and geometric calibration," *IEEE Trans. Geosci. Remote Sens.*, vol. 47, no. 12, pp. 3915–3932, Dec. 2009.
[22] A. Takeshiro, T. Furuya, and H. Fukuchi, "Verification of polarimetric calibration method including Faraday rotation compensation using PALSAR data," *IEEE Trans. Geosci. Remote Sens.*, vol. 47, no. 12, pp. 3960–3968, Dec. 2009.
[23] R. Touzi and M. Shimada, "Polarimetric PALSAR calibration," *IEEE Trans. Geosci. Remote Sens.*, vol. 47, no. 12, pp. 3951–3959, Dec. 2009
[24] A. Freeman, "SAR calibration: An overview," *IEEE Trans. Geosci. Remote Sens.*, vol. 30, no. 11, pp. 1107–1121, Nov. 1992.
[25] S. Quegan, "A unified algorithm for phase and cross-talk calibration of polarimetric data-theory and observations," *IEEE Trans. Geosci. Remote Sens.*, vol. 32, no. 1, pp. 89–99, Jan. 1994.
[26] M. Shimada, "Model-based polarimetric SAR calibration method using forest and surface-scattering targets," *IEEE Trans. Geosci. Remote Sens.*, vol. 49, no. 5, pp. 1712–1733, May 2011.
[27] P. López-Dekker *et al.*, "BIOMASS end-to-end mission performance simulator," in *Proc. IEEE IGARSS*, Vancouver, BC, Canada, 2011, pp. 4249–4252.
[28] M. J. Soja, G. Sandberg, and L. M. H. Ulander, "Regression-based retrieval of boreal forest biomass in sloping terrain using P-band SAR backscatter intensity data," *IEEE Trans. Geosci. Remote Sens.*, vol. 51, no. 5, pp. 2646–2665, May 2013.
[29] J.-S. Lee, D. L. Schuler, and T. L. Ainsworth, "Polarimetric SAR data compensation for terrain azimuth slope variation," *IEEE Trans. Geosci. Remote Sens.*, vol. 38, no. 5, pp. 2153–2163, Sep. 2000.
[30] J. Nocedal and S. J. Wright. *Numerical Optimization*, 2nd ed. Berlin, Germany: Springer-Verlag, 2006, ser. Springer Series in Operations Research.

Shaun Quegan (M'90) received the B.A. and M.Sc. degrees in mathematics from the University of Warwick, Coventry, U.K., in 1970 and 1972, respectively, and the Ph.D. degree from the University of Sheffield, Sheffield, U.K., in 1982.

From 1982 to 1986, he was a Research Scientist with the Marconi Research Centre, Great Baddow, U.K., where he led the Remote Sensing Applications Group from 1984 to 1986. In 1986, he established the SAR Research Group at the University of Sheffield, where he became a Professor in 1993. In the same year, he helped inaugurate the Sheffield Centre for Earth Observation Science, University of Sheffield. In 2001, he became the Director of the U.K. National Environmental Research Council Centre for Terrestrial Carbon Dynamics. This multiinstitutional center was concerned with assimilating Earth observation (EO) and other data into the process models of the land component of the carbon cycle and now forms part of the U.K. National Centre for Earth Observation. His broad interests in the physics, systems, and data analysis aspects of radar remote sensing are now subsumed in the more general aim of exploiting many sorts of EO technology to give greater quantitative understanding of the carbon cycle.

Mark R. Lomas received the B.Sc. and Ph.D. degrees in applied and computational mathematics from the University of Sheffield, Sheffield, U.K., in 1989 and 1995, respectively. His Ph.D. studies investigated the phenomenon of voltage collapse.

Since 1994, he has been a Research Associate with the Department of Animal and Plant Science and the School of Mathematics and Statistics, University of Sheffield, where he mainly works on the global land surface carbon and hydrological cycles via dynamic vegetation models, specifically the Sheffield Dynamic Global Vegetation Model and its predecessor, the Dynamic Global Phytogeography (DOLY) model, which he played a key role in developing. A large part of his research has been concerned with utilizing Earth, the observation data to test and improve these models.

Dr. Lomas' Ph.D. studies were funded by the National Grid.